

Physics-informed hierarchical data-driven predictive control for building HVAC systems to achieve energy and health nexus

Xuezheng Wang, Bing Dong*

Department of Mechanical & Aerospace Engineering, Syracuse University, 263 Link Hall, Syracuse, NY 13244, United States



ARTICLE INFO

Keywords:

Model predictive control
Physics-informed neural network
Energy reduction
Indoor environmental quality

ABSTRACT

Buildings consume 74% of US electricity and 40% of primary energy use. However, 15% of the energy was wasted due to bad controls. Many research studies have demonstrated that model predictive control strategies could provide significant energy savings, but the lack of a scalable building dynamic model impeded the large-scale implementation of predictive control strategies. Moreover, many predictive control strategies lacked the consideration of indoor air quality. Therefore, in this research study, we proposed a novel physics-informed input convex neural network (PINN) to predict indoor environmental dynamics with 6 h ahead. The model sanity check results showed that the proposed PINN had physically consistent behavior to different control inputs. Then, the PINN is used to design a hierarchical data-driven predictive control (HDDPC) strategy to minimize both the space cooling load and airside coil load. Three different case studies were simulated to evaluate the proposed control strategy comprehensively: a) maintaining a similar indoor temperature profile as the measurement to evaluate energy reduction potential by the HDDPC; b) evaluating the impact of the proposed weather forecast models on the HDDPC performance by comparing the case with perfectly accurate weather information and the case with forecasted weather information. Results indicated that the hierarchical data-driven predictive control strategy with weather forecasting had a similar performance with measured weather inputs. On average, the HDDPC strategy could reduce more than 35% of total cooling energy and 70% of total airside coil energy with the guarantee of indoor thermal comfort and air quality.

1. Introduction

1.1. Motivation

In the U.S., the building sector accounts for 74% of electricity use and 40% of primary energy use [1]. Within the building sector, commercial building heating, ventilating, and air conditioning (HVAC) system contributes to more than 410 billion kWh of energy usage [2] and generates 16 percent of all U.S. carbon dioxide emissions [3]. However, 30% of the energy was wasted [4] and 15% of the energy was wasted due to building control [5]. One of the reasons for such a large waste is that the indoor environment is affected by many factors such as outdoor temperatures, solar radiation, occupants, and thermal lagging effect, but most control strategies do not consider all factors above and only react with current sensor readings. Therefore, improving energy efficiency and decarbonizing buildings are of great importance because it has a tremendous positive impact on our environment and energy security [6]. Developing an advanced control strategy for the commercial HVAC

system is crucial for achieving the goals.

Every day, people spend more than 90% of their time indoors [7]. Indoor environmental quality is of great importance to people's mental and physical health. Thermal comfort and indoor air quality are two typical indices of indoor environmental quality. To maintain indoor environmental quality, indoor temperatures need to be in a comfortable range to ensure thermal comfort, and indoor contaminant concentrations need to be under the threshold for good indoor air quality. Among many types of indoor contaminants, carbon dioxide is mostly used to quantify indoor air quality not only because of economical sensors off the shelf but also due to its nexus with other indoor contaminants [8]. After the pandemic of coronavirus disease 2019, extended time indoors made people pay more attention to their indoor environment, which led to more strict ventilation suggestions from CDC and EPA [9,10].

HVAC systems are primarily used to regulate indoor environments and account for great portions of building energy usage. Therefore, advanced control strategies for HVAC systems will mitigate the energy-wasting issue greatly for the building sector. Among many advanced

* Corresponding author.

E-mail address: bidong@syr.edu (B. Dong).

control strategies, model predictive control is the most promising because of its ability to consider multiple objectives. Research has indicated that model predictive control could provide 20 ~ 40% energy savings while maintaining good indoor environmental quality in different climate zones [11].

Traditional model-based predictive control requires robust predictive models, which are typically developed based on physics. The physical parameters help the model's accuracy. However, buildings are different from each other, and the types of HVAC systems are also different. Parameters of physics-based models would vary greatly and require domain expertise to develop even with the auto-tuning process, which impedes the adoption of model-based predictive control on a large scale. With the development of machine learning techniques, purely data-driven models provide great potential for scalable predictive models. In addition, most data-driven models lack the physical meaning of variables, which is important for building controls. Furthermore, many advanced control strategies aimed at improving energy efficiency will sacrifice comfort and indoor air quality, which will result in a loss of productivity.

Therefore, this paper aims to develop a predictive-control-oriented data-driven model with physically interpretable behaviors and a hierarchical predictive control strategy to balance HVAC system energy usage, thermal comfort, and indoor air quality.

1.2. Literature review

In recent years, incorporating machine learning approaches into optimal control strategies started to emerge in different studies. According to the literature review, machine learning approaches were mostly used to 1) be a surrogate of the objective function [12,13], 2) decompose the optimal variables to low-level writable points in the control system [12], 3) learn an agent-like control policy [14,15,16], and 4) replace the system dynamic models [14,15,16,17,18,19,20,21,22,23,24,25].

Among the four aforementioned aspects, most research studies focused on developing data-driven system dynamic models. Specifically, for optimal control of indoor environments, [24] developed two ANN models to forecast indoor dynamics and thermal comfort. The models were coupled into a multi-objective MPC to balance energy cost and thermal comfort. Although the experiment demonstrated the performance of the proposed MPC strategy, the ANN models were not constructed to guarantee convexity, so the authors had to use a hybrid solver to avoid local optima.

In other studies, the data-driven models were developed as either physics-informed or input convex. Inspired by the one-step state-space model, the authors in [14,15] proposed a neural state-space structure. The neural networks were developed to replace the state, control, disturbance, and output terms. Moreover, a recurrent architecture was used for multi-step prediction. Similarly on the inspiration but differently in the approach, the authors in [16] incorporated physics-informed terms in the loss function to force a physically consistent behavior for the neural network. In both studies, the authors did not directly tackle the optimization problem. Instead, in the first few studies [14,15], the authors used the neural network with an MPC-inspired loss function to learn a differentiable control law, while the authors in the second study developed a reinforcement learning framework to facilitate optimal control [17]. Another physics-informed neural network developed by [18] consists of two multi-step predictors. An encoder-LSTM-decoder model predicted unforced thermal dynamics. A physics-inspired model predicted energy accumulation in the building. The combining output from two predictors gave actual indoor temperature predictions. The neural network outperformed the RC model with physically consistent predictions, but no control strategy was developed accordingly.

As for convex approaches, Bünnig et al. represented indoor thermal dynamics using a random forest with linear regression [19], input

convex neural network [20], and physics-informed linear regressor [21]. Since both models and problems were formulated to be convex, the authors directly solved optimization problems for predictive control strategies. The experiments demonstrated the control performance with significant savings in heating and cooling load. However, recurrent architecture was used for multi-step prediction, and indoor air quality and system level energy usage was not considered in the predictive control strategies.

1.3. Research gaps and contributions

Many research studies have demonstrated that model predictive control strategies have a great performance in balancing building energy cost and indoor comfort [26,27,28,29,30,31,24,32,33,34,35]. However, it needs much expertise to develop, especially to develop a control-oriented model. Researchers reported that the model development typically takes 79 person-days, which accounts for 33% of the total effort required for the implementation and operation of MPC [36]. A scalable model is needed for the large-scale implementation of MPC strategies.

Some data-driven models were proposed in research studies as a surrogate of indoor thermal dynamic models. Such models tend to predict one-step-ahead indoor dynamics. However, in predictive control strategies, multiple-step-ahead predictions are needed, which requires a recurrent architecture for one-step-ahead prediction models. The recurrent structure will cause gradient vanishing and explosion issues and hence degrade the performance for long prediction horizons [15]. According to [20], as the prediction horizon increased from 1 h to 6 h, the mean squared prediction error increased from less than 0.2 °C to more than 1 °C. Another research using the recurrent neural network (RNN) [15] indicated that models with RNN blocks tend to have good performance for short horizons, but multilayer perceptron (MLP) models score better when prediction steps are more than 64 for their case. The reason can be explained by unrolling the RNN. For example, for the last point in the prediction sequence of the next 6-hour indoor temperature with 15-minute time intervals, using a 3-layer RNN model is equivalent to using a 72-layer MLP. The same weight will be multiplied over and over across the prediction steps, which causes the recurrent structure prone to gradient explosion and vanishing problems. Although the issue can be addressed by the LSTM structure, the convexity of the model and therefore optimal solutions cannot be guaranteed due to non-convex activation functions in the gates. Therefore, a convex data-driven model without a recurrent architecture is needed for the multi-step prediction of indoor dynamics.

To our best knowledge, most research studies related to data-driven prediction control (DDPC) focused on the space load only. The energy usage on the system level was hardly considered. The space load reduction would indirectly affect system energy usage in terms of supply airflow rate and supply air temperature. However, fresh air intake also contributes to a great portion of system energy consumption, which is not reflected in the space load. Moreover, to consider system-level energy usage, it is inevitable to consider indoor air quality because supply and fresh airflow directly affect it, which was not considered in aforementioned studies. Therefore, the exploration of data-driven predictive control on both room and system levels is necessary for more potential energy savings; and a control-oriented data-driven model was developed in this study to describe the dynamic of indoor air quality and coupled into the data-driven predictive control strategy to avoid sacrifice of indoor air quality while saving energy.

Lastly, the impact of weather forecasts on data-driven predictive control performance was not analyzed in previous research studies. Inaccurate weather forecasts would lead to overestimation or underestimation of space load and ventilation rate, which would result in sub-optimal energy savings. Meanwhile, inaccurate weather forecasts and suboptimal space load have a combined effect on system energy usage, which was also not analyzed in previous studies. A comparison of ideal

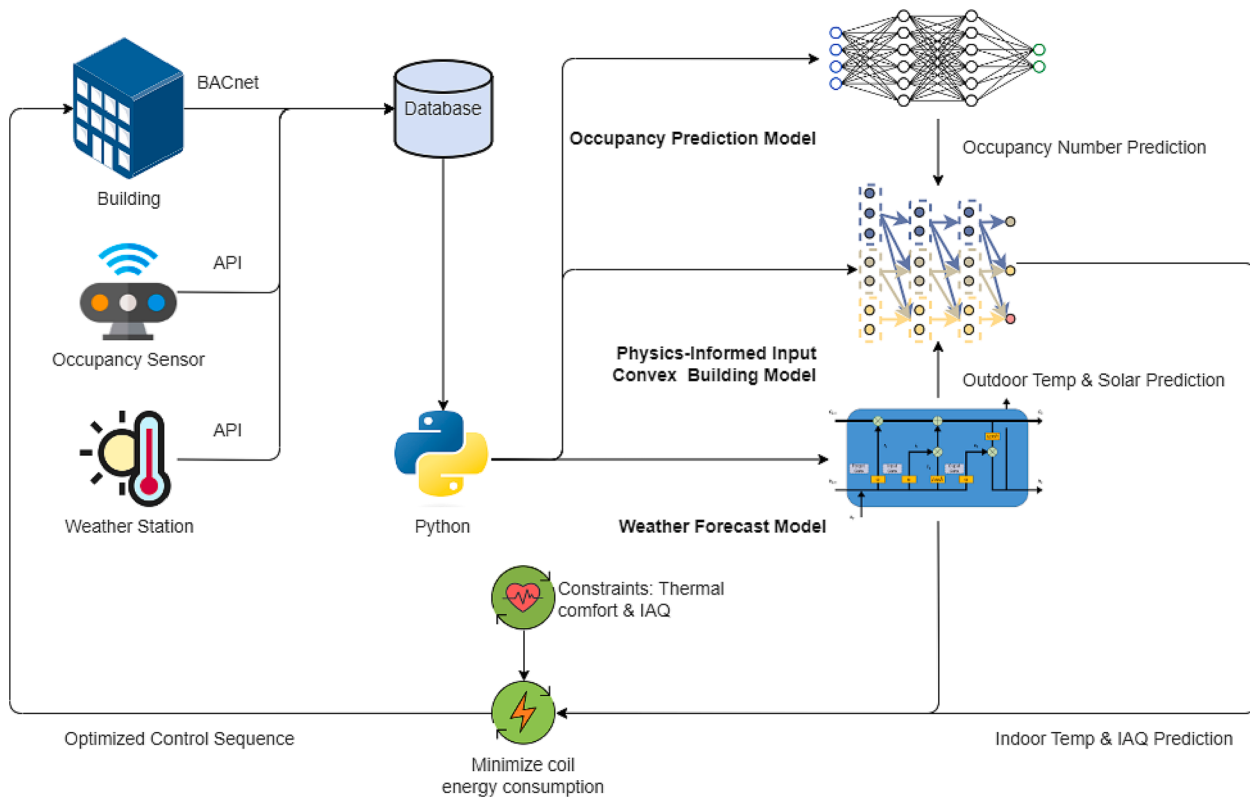


Fig. 2-1. Overall framework of data-driven predictive control strategy.

and realistic situations is needed for a better understanding of data-driven predictive control performance.

In summary, current research gaps of data-driven predictive control for building systems are:

1. Most DDPC-related research studies used recurrent neural networks which are prone to performance degradation for long prediction horizons. The non-recurrent models are not explored.
2. Most DDPC-related research studies only considered indoor temperature as an index for the indoor environment. Indoor air quality, as another important index, is hardly considered.
3. Most DDPC-related research studies only considered space cooling or heating load. The load of coils is hardly considered.
4. The impact of the weather forecast on the DDPC performance is important but lacking in research.

Therefore, the scientific contributions of this paper are:

1. Developing an ANN-based, physics-informed, multi-step prediction model for indoor dynamics.
2. Incorporating indoor CO₂ concentration and coil load into DDPC strategy.
3. Proving convexity of the proposed control strategy.
4. Comprehensive analysis of the proposed DDPC strategy in different simulation scenarios.
5. Comprehensively analysis the weather forecast impact and correlation between different control levels.

The rest of the article is organized as follows. In section 2, we introduced our physics-informed neural network and how to evaluate its performance. The convex HDDPC strategy was also formulated and proved in this section. In section 3, we presented and discussed case study results. The limitation and potential improvements were discussed in section 4. We concluded in section 5.

2. Methodology

The overall framework is shown in Fig. 2-1. Each part of the framework is explained in detail in the following.

Nomenclature

<i>Symbols</i>	
<i>A</i>	State matrix
<i>B</i>	Input matrix
<i>E</i>	Disturbance matrix
<i>h</i>	Prediction horizon
<i>x</i>	State variable
<i>u</i>	Control variable
<i>W</i>	Disturbance variable
<i>t</i>	Time step
<i>z</i>	Output from neural network layers
<i>g</i>	Activation function
<i>w</i>	Weight of neural network
<i>j</i>	Layer of the neural network
\hat{y}	Prediction from neural network
<i>P</i>	Load
<i>T</i>	Temperature
<i>f</i>	Neural network function
\dot{Q}	Volumetric airflow rate
<i>c_p</i>	Specific heat of air
ρ	Air density
<i>C</i>	Concentration
<i>Accents</i>	
-	Upper bound
-	Lower bound
<i>Subscripts</i>	
\bullet_{out}	Outdoor air
\bullet_{sup}	Supply air
\bullet_{room}	Room air
\bullet_{set}	Setpoint
<i>Abbreviations</i>	
PINN	Physical-informed neural network
HDDPC	Hierarchical data-driven predictive control

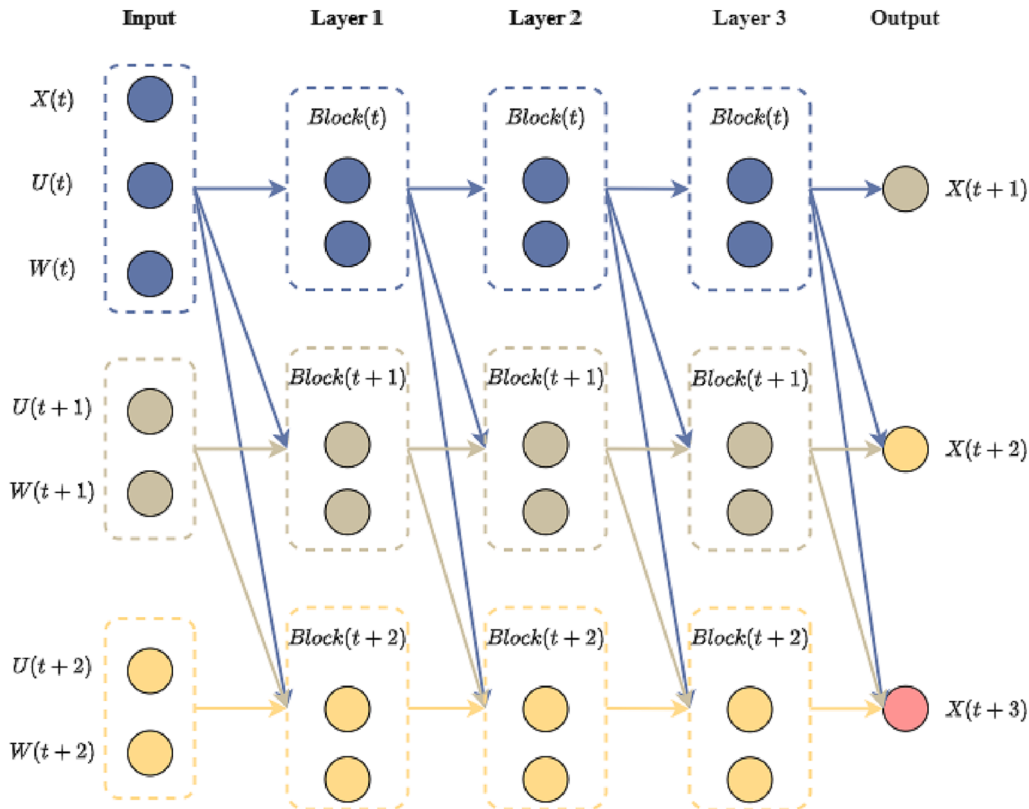


Fig. 2-2. Masked neural network.

2.1. Development of a Physics-informed input convex neural networks model

Gray-box models are widely used in model predictive control strategies. In our previous study, a physics-based 3R2C building thermal model was used to predict indoor temperature changes in a student office [11]. Meanwhile, the physics-based indoor air quality model was developed and linearized to a state-space representation and coupled with the building thermal model.

However, as the physics-based model requires expertise to develop and vanilla black-box models were not designed for control purposes, in this study, we proposed a control-oriented data-driven model inspired by the structure of the physics-based model.

A general form of the coupled one-step model is $x(t+1) = Ax(t) + Bu(t) + EW(t)$, where x , u , and W are state, controllable, and disturbance variables, respectively; A , B , and E are coefficient matrices. For predictive control purposes, the one-step state-space model was reformed as a multi-step state-space model:

$$x(t+1 : t+h) = A_h x(t) + B_h u(t : t+h-1) + E_h W(t : t+h-1) \quad (1)$$

Where h is the prediction horizon; A_h , B_h , E_h and are obtained based on coefficient matrices and expressed as:

$$A_h = [A \quad A^2 \quad \dots \quad A^h]^T$$

$$B_h = \begin{bmatrix} B & 0 & \dots & 0 \\ AB & B & \dots & 0 \\ \vdots & \vdots & \ddots & \vdots \\ A^{h-1}B & A^{h-2}B & \dots & B \end{bmatrix}$$

$$E_h = \begin{bmatrix} E & 0 & \dots & 0 \\ AE & E & \dots & 0 \\ \vdots & \vdots & \ddots & \vdots \\ A^{h-1}E & A^{h-2}E & \dots & E \end{bmatrix}$$

When solving the optimization problem in each control step, the multi-step state-space model, rather than the one-step state-space model, plays the key role of predicting indoor environmental dynamics. Therefore, this research seeks to use a black-box model as a surrogate of the multi-step state-space model. Because the matrices B_h and E_h are lower triangular, for each control time step, the prediction of the next step only relates to historical and current control and disturbance variables. Inspired by such nature, we propose a partially connected neural network to predict indoor dynamics.

In the partially connected neural network, the neurons of each layer were separated into different blocks. Each block represents different time steps and only contains information no more than this time step. In other words, each block only leverages current and historical information and contains no future information. To achieve this characteristic, each block needs to be connected in a special way which forces the weights related to future information to be zeros. By this means, the neural network was partially connected. We call it a masked neural network because some neurons are ‘masked’ with respect to certain neurons.

More specifically, the connection between different layers can be formulated as follows:

For the first layer,

$$\begin{bmatrix} z_1(t) \\ z_1(t+1) \\ z_1(t+2) \\ \vdots \\ z_1(t+h-1) \end{bmatrix} = g_1 \left(w_1 \begin{bmatrix} x(t) \\ u(t) \\ u(t+1) \\ \vdots \\ u(t+h-1) \end{bmatrix} \right) \quad (2)$$

Where $z_1(i)$ ($i \in [t, t+h-1]$) is the output of the block in the 1st

layer that contains information no more than the i th time step, which can contain a certain number of neurons; g_1 is the activation function of the first layer.

Different from fully connected neural networks, the weight matrix of the first layer, w_1 , is expressed as:

$$w_1 = \begin{bmatrix} w_{t,x_t,1} & w_{t,u_t,1} & 0 & 0 & \cdots & 0 \\ w_{t+1,x_t,1} & w_{t+1,u_t,1} & w_{t+1,u_{t+1},1} & 0 & \cdots & 0 \\ w_{t+2,x_t,1} & w_{t+2,u_t,1} & w_{t+2,u_{t+1},1} & w_{t+2,u_{t+2},1} & \cdots & 0 \\ \vdots & \vdots & \vdots & \vdots & \ddots & \vdots \\ w_{t+h-1,x_t,1} & w_{t+h-1,u_t,1} & w_{t+h-1,u_{t+1},1} & w_{t+h-1,u_{t+2},1} & \cdots & w_{t+h-1,u_{t+h-1},1} \end{bmatrix}$$

Where $w_{i,...,1}$ is the weight related to the i th block of the 1st layer. The ‘masked’ weight matrix allows the neurons in each block to leverage only current and historical information.

Similarly, for hidden layers:

$$\begin{bmatrix} z_j(t) \\ z_j(t+1) \\ z_j(t+2) \\ \vdots \\ z_j(t+h-1) \end{bmatrix} = g_j \left(w_j \begin{bmatrix} z_{j-1}(t) \\ z_{j-1}(t+1) \\ z_{j-1}(t+2) \\ \vdots \\ z_{j-1}(t+h-1) \end{bmatrix} \right) \quad (3)$$

Where $z_j(i)$ is the output of the block in the j th layer that contains information no more than the i th time step; and g_j is the activation function of the j th layer.

The weight matrix of the j th layer, w_j , is expressed as:

$$w_j = \begin{bmatrix} w_{t,z_{t,j-1},j} & 0 & 0 & \cdots & 0 \\ w_{t+1,z_{t,j-1},j} & w_{t+1,z_{t+1,j-1},j} & 0 & \cdots & 0 \\ w_{t+2,z_{t,j-1},j} & w_{t+2,z_{t+1,j-1},j} & w_{t+2,z_{t+2,j-1},j} & \cdots & 0 \\ \vdots & \vdots & \vdots & \ddots & \vdots \\ w_{t+h-1,z_{t,j-1},j} & w_{t+h-1,z_{t+1,j-1},j} & w_{t+h-1,z_{t+2,j-1},j} & \cdots & w_{t+h-1,z_{t+h-1,j-1},j} \end{bmatrix}$$

Where $w_{i,...,j}$ is the weight related to the i th block of the j th layer.

Lastly, for the output layer:

$$\begin{bmatrix} x(t+1) \\ x(t+2) \\ x(t+3) \\ \vdots \\ x(t+h) \end{bmatrix} = g_o \left(w_o \begin{bmatrix} z_j(t) \\ z_j(t+1) \\ z_j(t+2) \\ \vdots \\ z_j(t+h-1) \end{bmatrix} \right) \quad (4)$$

The weight matrix of the output layer, w_o , is expressed as:

$$w_o = \begin{bmatrix} w_{t,z_t,j} & 0 & 0 & \cdots & 0 \\ w_{t+1,z_t,j} & w_{t+1,z_{t+1},j} & 0 & \cdots & 0 \\ w_{t+2,z_t,j} & w_{t+2,z_{t+1},j} & w_{t+2,z_{t+2},j} & \cdots & 0 \\ \vdots & \vdots & \vdots & \ddots & \vdots \\ w_{t+h-1,z_t,j} & w_{t+h-1,z_{t+1},j} & w_{t+h-1,z_{t+2},j} & \cdots & w_{t+h-1,z_{t+h-1},j} \end{bmatrix}$$

Note that in the formulation and this study, biases were not considered.

To be more explicit, the graphical interpretation is shown in Fig. 2-2. In the input layer, the disturbances W are also included as features. In essence, disturbances can be treated in the same way as input variables. Therefore, including disturbances does not cause the loss of generality for the aforementioned formulations. Using the aforementioned weight matrices, partial connections can be achieved in each layer. Block t of Layer 1 contains the information of the t th timestamp, which are current values of the state, input, and disturbance variables, while Block $t+1$ of Layer 1 contains the information of the t th and $t+1$ th time steps and so on. In the hidden layers, each block receives current and historical information. Exemplifying by Block $t+2$ of Layer 3, it receives outputs of Blocks t , $t+1$, and $t+2$ in Layer 2, which come from corresponding outputs from Layer 1 and hence input features. Lastly, in the output layer, the prediction of $x(t+2)$ is calculated based on the value of $x(t)$, $u(t)$, $W(t)$, $u(t+1)$, $W(t+1)$ from inputs, which indicates that future control inputs and disturbances have no effect on its value. Such characteristics embedded physical information into the neural network. For example, the outdoor temperature at 6:00 PM does not affect the indoor

temperature at 1:00 PM of the same day. If the neural network is fully connected, this nature does not hold anymore, which indicates that all future inputs affect the prediction of a given time step which is not true in the actual indoor temperature dynamics. Moreover, to facilitate optimization, the weight of each neuron was set as a non-negative value. The activation function was selected to be convex. In this research study, the ReLU activation function was used. Such, the neural network is constructed as an input convex neural network [20].

In this study, two neural networks are developed to predict the indoor temperature and CO₂ concentration, respectively, for the next 6 h with 15-min time intervals. The input features of the neural networks are the same as the variables of physics-based models.

For indoor temperature prediction neural network, the input features include:

- Indoor temperature measurement at the current time step (one point)
- A sequence of HVAC load from the current time step to the next prediction horizon (24 points)
- A sequence of outdoor air temperature from the current time step to the next prediction horizon (24 points)
- A sequence of solar radiation from the current time step to the next prediction horizon (24 points)
- A sequence of occupancy numbers from the current time step to the next prediction horizon (24 points)

For indoor CO₂ prediction neural network, the input features are:

- Indoor CO₂ measurement at the current time step (one point)
- A sequence of outdoor airflow rate from the current time step to the next prediction horizon (24 points)
- A sequence of occupancy numbers from the current time step to the next prediction horizon (24 points)

The outputs of the two neural networks are sequences of indoor temperature and CO₂ predictions for the next prediction horizon (24 points each), respectively.

2.2. Model sanity check

Even though the neural networks were formed to be physics-informed and convex with respect to inputs, they still need to be tested to guarantee the control performance. The model sanity check includes three parts:

- Effect of accumulative errors:** in a real implementation and model training, the prediction of next-h-hour indoor temperature and CO₂ was based on the current measurement, along with control inputs and disturbances. However, in a simulation environment, such measurement was not included. Instead, the model prediction was treated as the response from the real environment and used recurrently in the next step, which would cause accumulative errors. Therefore, the model performance under such a recurrent process needs to be tested.
- Responses to control inputs:** we need to check whether the neural networks have reasonable responses to different control inputs. For example, the indoor air temperature and CO₂ prediction should be higher (lower) than the measurement if less (more) cooling load (fresh air) was provided. On the other hand, the effects of future inputs on the current time step prediction need to be tested by different scenarios.
- Response to disturbances:** Lastly, we also need to check the response of neural networks with different disturbance inputs. For the indoor air temperature neural network, the prediction should respond physics-consistently with disturbances.

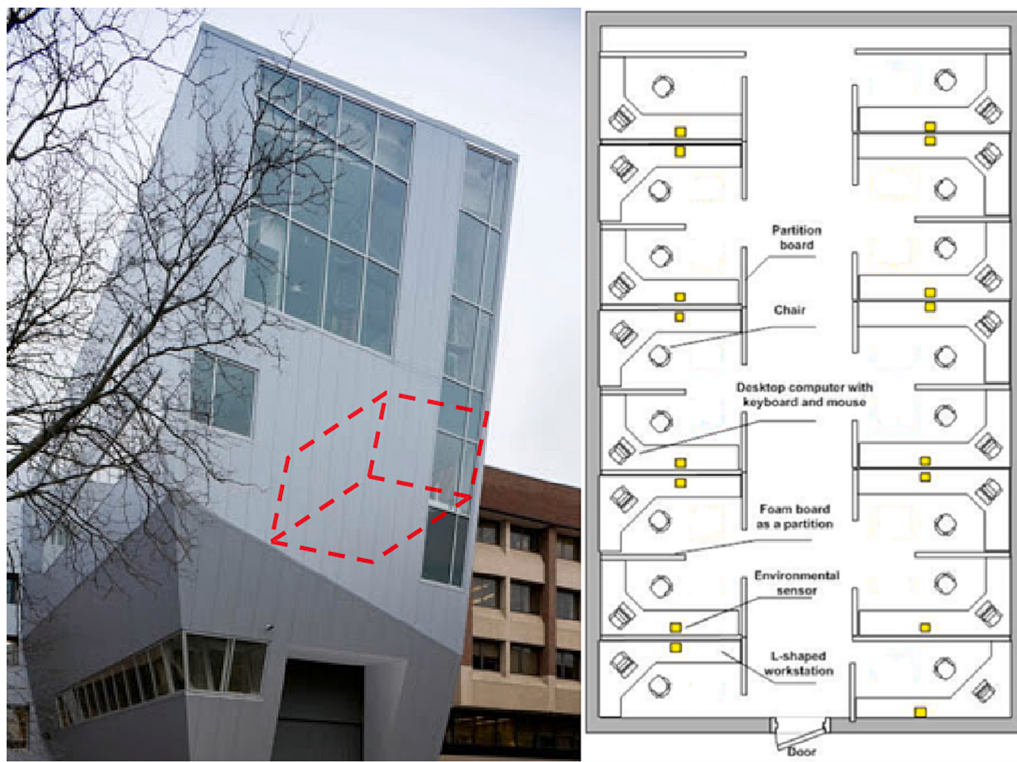


Fig. 2-3. Outside and plan views of the testbed.

Therefore, in this study, the model sanity was checked by following cases with different scenarios:

1. All input features are the same as measurement, except that the input indoor state values were from previous time step.
2. The control inputs were increased or decreased by a certain amount. Different scenarios were tested in each case. In the first scenario, all control inputs were changed. In the second scenario, the first control input was the same as the measurement, but the remaining control inputs were changed, and so on. In the last scenario, the control inputs were the same as the measurement except for the last one. Different scenarios were to test if future inputs have effects on the prediction for the current time step.
3. It is essentially the same as the second model sanity check, but instead of control inputs, disturbance inputs were changed.

2.3. Weather forecasting

Weather forecast with the same time interval as control frequency is needed for predictive control strategies. In this study, the control frequency is 15 min, and the prediction horizon is 6 h. At each control time step, a sequence of next-6-hour weather needs to be predicted. However, the highest weather forecast frequency available online is hourly, which cannot meet control purposes. Moreover, as a key impact factor of indoor environment, solar radiation forecast is hardly provided. Therefore, weather forecast models need to be developed for the proposed predictive control strategy. Prior research studies show that LSTM neural networks are widely used for weather forecasting and have better performance compared to the ANN models [37,38]. Therefore, two LSTM neural networks were developed to forecast outdoor air temperature and solar radiation for this study.

Specifically, for the outdoor temperature LSTM model, the input features were historical outdoor temperature and solar radiation, time of the day, and day of the year. For the solar radiation LSTM model, the input features were historical solar radiation, time of the day, and day of

the year. The outputs were forecasts for the next h hours with 15-minute time intervals. In this study, 6 h was the prediction horizon. The input sequence lengths were 6 h for the temperature forecast model, and 3 days for the solar radiation forecast model. Both models had two LSTM layers with 50 neurons. The loss function was MSE loss for the outdoor temperature LSTM model. For the solar radiation LSTM model, the loss function had an additional term to penalize negative predictions:

$$\text{Loss} = \text{MSE} + \sum (-\min(\hat{y}, 0)) \quad (5)$$

The weather data was acquired from Syracuse University Weather Station. Two-year data of 2019 and 2020 was used to train the models, and the first half-year data in 2021 was used for testing.

2.4. Develop a hierarchical data-driven predictive control framework

Based on data-driven indoor dynamic and weather forecasting models, a hierarchical data-driven predictive control (HDDPC) strategy was developed for the HVAC system. The room and system descriptions were the same as the ones in our previous study [11] (Fig. 2-3). In short, it was a small student office with an air handler unit and four VAVs. In this study, four VAVs were aggregated, and therefore the office was treated as a single zone.

In this study, due to the consideration of indoor air quality, the system-level energy usage should be considered as well. Because the indoor CO₂ is diluted mainly by the outdoor air intake, but the load that needs to condition the outdoor air cannot be reflected in the load to the space. Therefore, the predictive control strategies had both room-level and system-level controls.

For the room-level predictive control strategy, the cooling load from the HVAC system was optimized with the constraints of indoor thermal comfort:

$$\min \left(\sum P_{\text{hvac}}^2 \right) \quad (6)$$

$$\text{s.t. } \underline{P}_{\text{hvac}} \leq P_{\text{hvac}} \leq \overline{P}_{\text{hvac}} \quad (7)$$

$$\underline{T}_{room} \leq \bar{T}_{room} = f_{room}(P_{hvac}) \leq \overline{T}_{room} \quad (8)$$

Where P_{hvac} is the cooling load from the HVAC system; T_{room} is indoor air temperature; $f_{room}(x)$ is the input convex neural network of indoor thermal dynamics. The lower and upper bars represent the lower and upper bounds, respectively.

After room-level optimization was solved, on the system level, the air-side coil load was optimized with the constraints of indoor air quality and system operation limits:

$$\min \left(\sum P_{coil}^2 \right) \quad (9)$$

$$\begin{aligned} s.t. \quad P_{coil} &= c_p \rho \dot{Q}_{sup} (T_{mix} - T_{sup}) \\ &= c_p \rho \dot{Q}_{out} (T_{out} - T_{room}) + c_p \rho \dot{Q}_{sup} (T_{room} - T_{sup}) \end{aligned} \quad (10)$$

$$\underline{\dot{Q}_{out}} \leq \dot{Q}_{out} \leq \overline{\dot{Q}_{out}} \quad (11)$$

$$\underline{\dot{Q}_{sup}} \leq \dot{Q}_{sup} \leq \overline{\dot{Q}_{sup}} \quad (12)$$

$$\underline{T_{sup}} \leq T_{sup} \leq \overline{T_{sup}} \quad (13)$$

$$C_{co2} = f_{co2} \left(\dot{Q}_{out} \right) \leq \overline{C_{co2}} \quad (14)$$

$$P_{hvac} = c_p \rho \dot{Q}_{sup} (T_{sup} - T_{set}) \quad (15)$$

Where P_{coil} is the air-side coil load; \dot{Q}_{out} , \dot{Q}_{sup} , and T_{sup} are outdoor airflow rate, total supply airflow rate, and supply air temperature, respectively, which are system-level optimal variables; c_p and ρ are specific heat and density of the air, respectively; T_{mix} and T_{out} are mixed and outdoor air temperature, respectively. As connections between system-level and room-level optimizations, T_{room} was treated as constants from room-level optimization, and P_{hvac} was calculated by supply temperature and airflow rate which are related with system-level optimal variables. To solve this optimization problem, the COBYLA algorithm from the SciPy package was used [39], which was the same as prior research studies [20,21].

2.5. Proof of convexity analysis for HDDPC

The local optima affected the performance of the predictive control strategy significantly. However, a convex optimization problem leads to global optima. To guarantee a global optimum, the hierarchical DDPC was used and approved convexity as follows.

For room-level optimization, the objective function was solely related to the cooling load without decomposition to any low-level variables. As for constraints, the lower and upper bounds of optimal variables were convex; and the room temperature constraints were also convex because the indoor thermal dynamic model was input convex. Therefore, room-level optimization is essentially a least square problem with convex constraint functions.

For system-level optimization, the equality constraint can be coupled into the objective function:

$$\sum P_{coil} = \sum c_p^2 \rho^2 \left[\dot{Q}_{out} (T_{out} - T_{room}) + \dot{Q}_{sup} (T_{room} - T_{sup}) \right]^2 \quad (16)$$

The system-level objective function is essentially the summation for the quadratic composition with affine mapping. Based on the operation that preserves convexity, the system-level objective function is a convex function.

Eliminating the variable T_{sup} by substituting the equality constraint (15) into (13):

$$\underline{T_{sup}} \leq \frac{P_{hvac}}{c_p \rho \dot{Q}_{sup}} + T_{set} \leq \overline{T_{sup}} \quad (17)$$

Which is a quasi-convex constraint function because the lower and upper contour sets are convex sets.

As for other constraint functions, constraints (11) and (12) are bounds and therefore convex constraints. The constraint (14) is constructed as input convex and therefore also a convex constraint. Therefore, the system-level optimization is a quasi-convex problem.

Because room-level and system-level optimizations were either convex or quasi-convex, the proposed hierarchical DDPC strategy could reach global optima when solutions were feasible.

2.6. Simulation case studies

To comprehensively evaluate the performance of the proposed HDDPC strategy, three simulation cases were studied.

Case 1: Evaluate energy reduction potential while tracking measured temperature dynamics. In this case, the constraints of both levels were as follows:

$$T_{measure} - 1^\circ C \leq T_{room} \leq T_{measure} + 1^\circ C$$

$$0.1 \dot{Q}_{sup} \leq \dot{Q}_{out} \leq 0.9 \dot{Q}_{sup}$$

$$0.22(480) \leq \dot{Q}_{sup} \leq 0.68(480) m^3 / s(CFM)$$

$$10(50) \leq T_{sup} \leq 18.3^\circ C (65^\circ F)$$

$$C_{co2} \leq 550 PPM$$

For indoor temperature difference, the $1^\circ C$ error bound was decided based on the temperature sensor error and model error. The bounds of supply airflow rate and temperature were based on system settings and actual measurement data. Based on industry-standard RESET [40], 600 PPM concentration for CO₂ provides occupants with high performance, which could be an upper bound for CO₂ concentration. However, from the CO₂ measurements, the indoor concentration hardly exceeded 600 PPM. Therefore, a strict CO₂ requirement of 550 PPM was given to test DDPC's performance in maintaining IAQ. As input features of physics-informed input convex neural networks, the measured outdoor weather data (both temperature and solar radiation) were used.

Case 2: Evaluate energy reduction potential with measured weather information while maintaining indoor temperature and CO₂ concentration in a range. Most constraints were the same as in the first case, except

$$21.1(70) \leq T_{room} \leq 23.8^\circ C (75^\circ F), 6:00 AM - 6:00 PM$$

$$18.3(65) \leq T_{room} \leq 26.7^\circ C (80^\circ F), \text{otherwise}$$

Case 3: Evaluate energy reduction potential with predicted weather information while maintaining indoor environmental quality. The third case was similar to the second case. However, weather forecasting from LSTM neural networks was used in input features. This case aimed to simulate a real implementation situation and test the robustness of the HDDPC with proposed weather forecast models.

3. Results and discussions

3.1. Model sanity check results

We used data measured from a student office to evaluate the performance of proposed neural networks and DDPC strategy. The measured data was collected every 5 min and resampled as 15 min and included indoor environmental information, weather information, and HVAC operational information.

Table 1Parameters of indoor temperature and CO₂ neural networks.

Model parameters	Indoor temperature model	Indoor CO ₂ model
Number of layers	3	3
Step to predict	24	24
Neurons for each block	40	20
Epochs	10e4	2e4
Initial training data set size	2016 points * 97 inputs	2016 points * 49 inputs
Training data set increment	96 points * 97 inputs	96 points * 49 inputs
Testing data set size	96 points * 97 inputs	96 points * 49 inputs

According to [21], the input convex neural network (ICNN) performance improved significantly with more than four-week training data. In this study, with the physics-informed structure, we found that starting from three-week training data could guarantee prediction errors less than sensor errors, which was 0.5 °C (0.9 °F) for temperature sensors and 50 PPM for CO₂ sensors. Since the indoor air quality data was available after June 23rd, 2021, we started our testing on July 14th, 2021. To mimic a real implementation, we increased the amount of training data by days as the testing date moved. Because students went on vacation after the week of August 13th, the simulation study stopped on August 13th. The input features of the indoor temperature model included the current step indoor temperature and 6 h, with a 15-minute resolution, of cooling loads, solar radiation, occupant numbers, and ambient temperature. The input features of the indoor CO₂ model were the current sensor reading and 6 h of fresh airflow rate and occupant number with the same time interval. The outputs of the two models were the next 6-hour indoor temperature and CO₂ concentration, respectively. The models were constructed with 3 hidden layers, with 40 and 20 neurons in each block, respectively for indoor temperature and CO₂ models. Table 1 shows parameters for the model development.

In the model training and testing, the input state values were from the measurement. However, in the simulation, we treated the response from indoor dynamic models as from the real indoor environment. Therefore, we first presented the results of the model sanity check case, in which the prediction was used as next-step input to evaluate

accumulative model errors during each testing day.

3.1.1. Model sanity check for actual control inputs

As shown in dark green lines in Fig. 3-1 and Fig. 3-2, indoor temperature and CO₂ concentration predictions on July 23rd followed the same trend as the measurement over different steps if the actual control input was used. Even without correction from measured data at each time step, the MAPE was around 1% for the temperature prediction and 4.2% for the CO₂ prediction. The absolute error of both kinds of predictions was within the sensor errors at the most time steps. Both models exhibited such performance on each testing day, and the overall model performance is listed in Table 2 and Table 3. The average indoor temperature prediction MAPE during the one-month test was around 1.1% for all prediction steps. The average MAE of indoor temperature prediction was around 0.44 °C (0.8 °F) for all prediction steps, which was less than the temperature sensor error (0.5 °C / 0.9 °F). On the other hand, the average indoor CO₂ prediction MAPE and MAE were around 4.7% and 21 PPM, respectively, which was also less than the sensor error (50 PPM).

3.1.2. Model sanity check for perturbed control inputs

For the model sanity check with more and fewer control inputs, we only present the results of July 23rd to illustrate, as shown in light green and orange lines in Fig. 3-1 and Fig. 3-2.

To check indoor temperature model responses, we gave 50% less and 100% more cooling loads in the aforementioned two cases, respectively. In each case, 24 scenarios were tested, in which different steps of cooling load were changed.

Case 1: Model response with less cooling loads. In the first plot of Fig. 3, in which all cooling loads were changed, indoor temperature deviated from measurement. The indoor temperature prediction increased significantly in the case without any cooling load. The maximum outdoor temperature was 26.7 °C (80 °F), and the maximum solar radiation was 1020 W/m² on July 23rd. Also considering internal heat gain from occupants and devices, such an increase was physically interpretable.

Case 2: Model response with more cooling loads. When 100% more cooling load was consistently given, the indoor air temperature

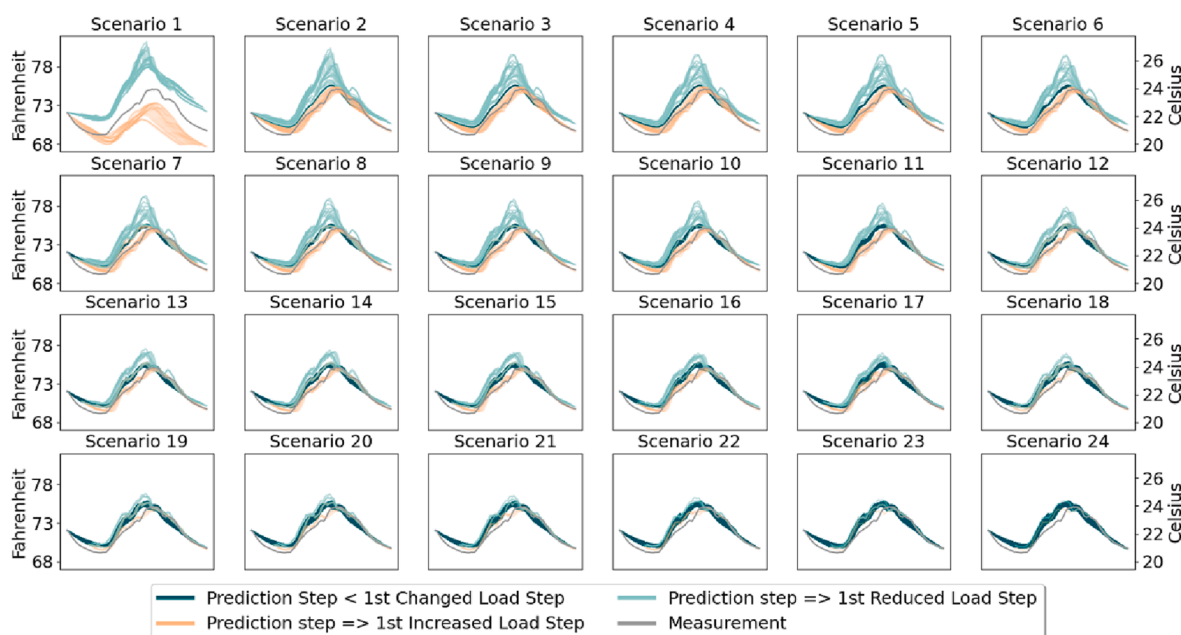


Fig. 3-1. Temperature model sanity check with different cooling loads on July 23rd. Light green lines were results with reduced cooling load. Orange lines were results with increased cooling load. Dark green lines were results with measured cooling loads. Grey lines were measurements. (For interpretation of the references to colour in this figure legend, the reader is referred to the web version of this article.)

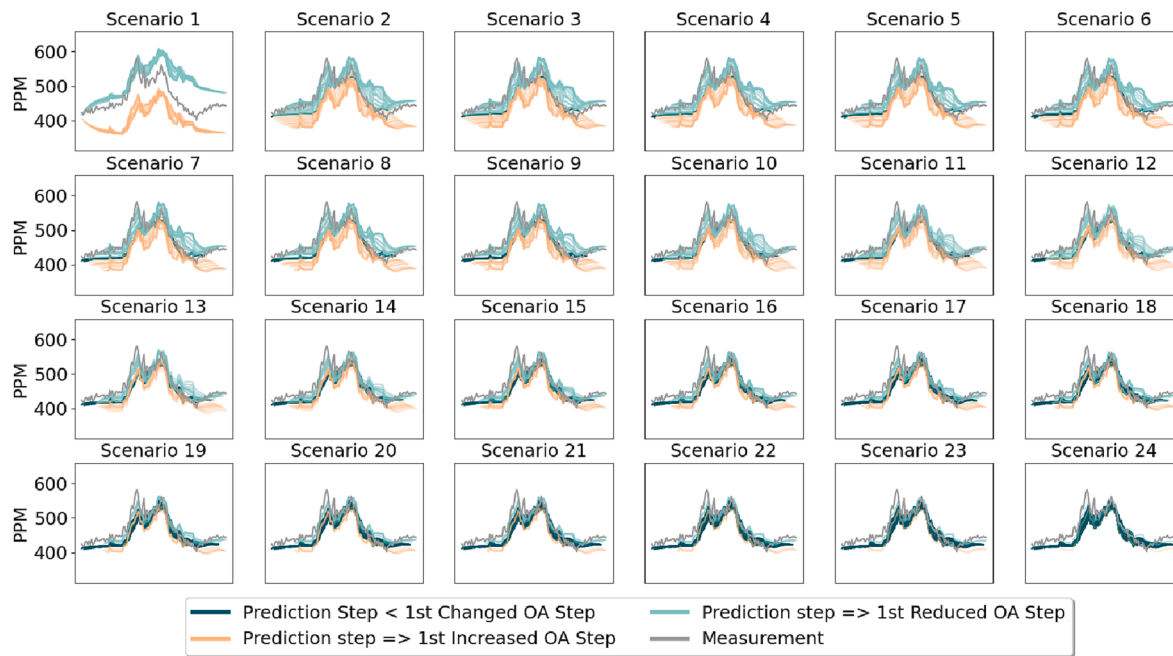


Fig. 3-2. CO₂ model sanity check with different outdoor airflow on July 23rd. Light green lines were results with reduced outdoor airflow. Orange lines were results with increased outdoor airflow. Dark green lines were results with original outdoor airflow. Grey lines were measurements. (For interpretation of the references to colour in this figure legend, the reader is referred to the web version of this article.)

Table 2

Average MAPE (%) and MAE (°C) of indoor temperature model of each step during the testing period.

Steps	1	2	3	4	5	6	7	8	9	10	11	12
MAPE	1.092	1.101	1.107	1.101	1.095	1.096	1.099	1.093	1.106	1.105	1.106	1.102
MAE	0.442	0.446	0.448	0.446	0.443	0.444	0.445	0.443	0.448	0.447	0.448	0.446
Steps	13	14	15	16	17	18	19	20	21	22	23	24
MAPE	1.105	1.105	1.107	1.116	1.125	1.123	1.112	1.106	1.095	1.104	1.099	1.093
MAE	0.448	0.447	0.449	0.453	0.457	0.456	0.452	0.451	0.444	0.448	0.446	0.443

Table 3

Average MAPE (%) and MAE (PPM) of indoor CO₂ model of each step during the testing period.

Steps	1	2	3	4	5	6	7	8	9	10	11	12
MAPE	4.642	4.676	4.7	4.709	4.714	4.704	4.735	4.755	4.767	4.779	4.79	4.795
MAE	21.853	21.99	22.09	22.126	22.135	22.088	22.238	22.354	22.426	22.48	22.521	22.563
Steps	13	14	15	16	17	18	19	20	21	22	23	24
MAPE	4.796	4.841	4.841	4.759	4.773	4.721	4.69	4.647	4.615	4.614	4.582	4.616
MAE	22.561	22.762	22.743	22.328	22.368	22.108	21.195	21.774	21.596	21.565	21.418	21.563

prediction decreased but not incredibly. For the scenarios in which the cooling load was not changed in the first certain steps, the corresponding temperature predictions converged the results with the measured cooling load.

For the indoor CO₂ model, 2 cases were tested with 24 different scenarios.

Case 1: Model response with more fresh airflow rate. For the case with more outdoor airflow rate, doubled fresh air was given. The indoor CO₂ prediction decreased with more outdoor airflow rate. Even with the maximum outdoor airflow rate, the indoor CO₂ predictions were still around 400 PPM, which was similar to the outside CO₂ concentration.

Case 2: Model response with less fresh airflow rate. On the other hand, when less outdoor air was given, the indoor CO₂ concentration increased during the day and reached a maximum of more than 600 PPM in the afternoon when there were 6 students in the office. When the fresh air flow rate was kept the same as the measurement in the first certain time steps, the corresponding CO₂ prediction was neither affected by the future fresh airflow rate, as shown in scenarios 2 to 24. Such behavior in

both models indicated that future control inputs didn't affect the prediction for the current steps, which validated our physics-informed model structure.

3.1.3. Model sanity check for disturbances

For the model sanity check with different disturbances, similarly, we present the temperature model response with increased (decreased) outdoor temperature and solar radiation, respectively, in Fig. 3-3 and Fig. 3-4. For the case with different outdoor air temperatures, we increased (decreased) measured values by 5.5 °C (10 °F), shown as light green (orange) lines in Fig. 3-3. Similarly, for the case with increased solar radiation, we increased measured values by 375 W per square meter and set the radiation to 0 in another case with decreased solar radiation, shown as light green and orange lines in Fig. 3-4, respectively. As indicated in the two figures, the indoor temperature model had physics-consistent predictions with different disturbances. Moreover, scenarios 2 to 24 indicated that the future outdoor temperature and solar radiation had no effect on the prediction of the current time step, which

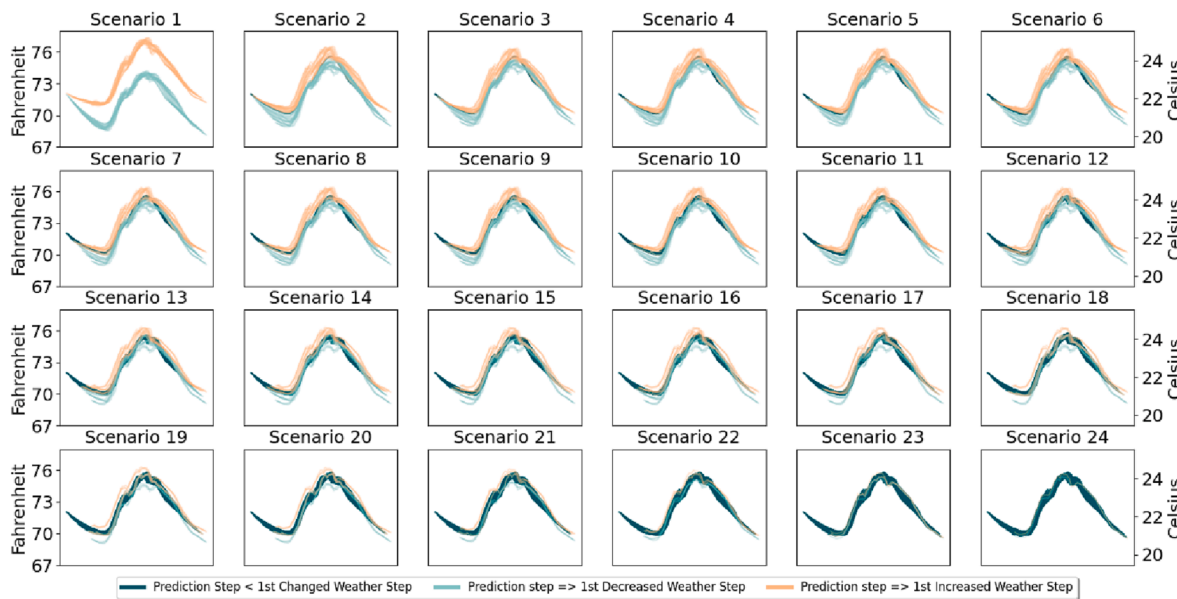


Fig. 3-3. Temperature model sanity check with different outdoor air temperature on July 23rd. Light green lines were results with decreased outdoor air temperature. Orange lines were results with increased outdoor air temperature. Dark green lines were results with measured outdoor air temperature. (For interpretation of the references to colour in this figure legend, the reader is referred to the web version of this article.)

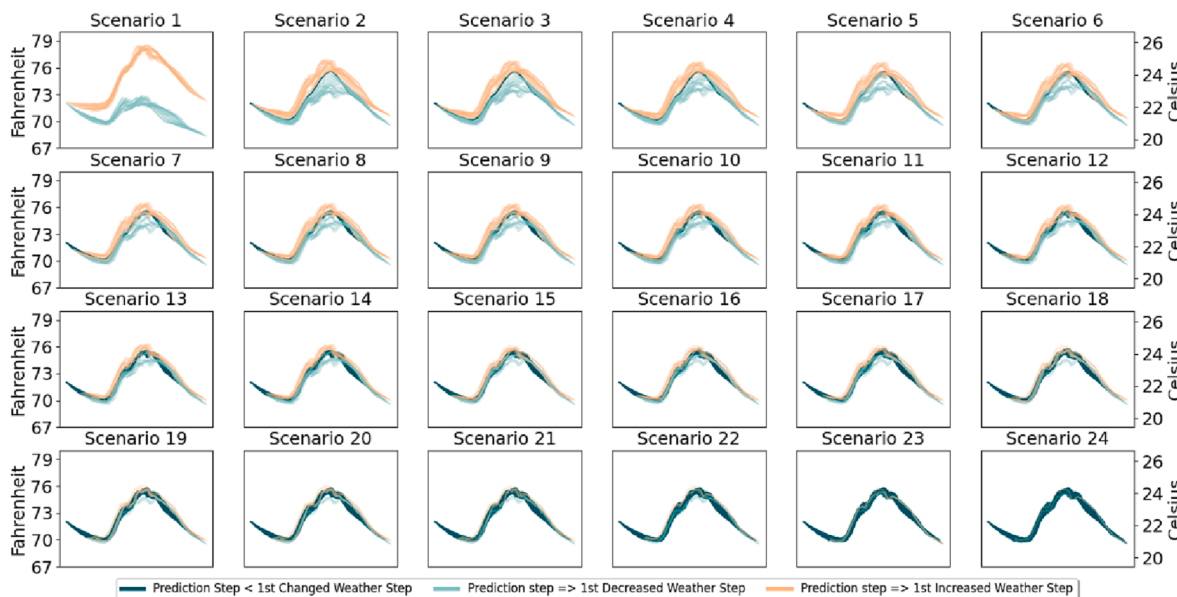


Fig. 3-4. Temperature model sanity check with different solar radiation on July 23rd. Light green lines were results with decreased solar radiation. Orange lines were results with increased solar radiation. Dark green lines were results with measured solar radiation. (For interpretation of the references to colour in this figure legend, the reader is referred to the web version of this article.)

validated our model structure.

In summary, the model prediction errors were within sensor errors for different prediction steps. Moreover, with different control inputs and disturbances at different prediction steps, the models had physically consistent responses, which benefited from physics-informed model structures. Therefore, in the study of the DDPC strategy, we treated the model outputs as responses from the real building environment.

3.2. Simulation results

3.2.1. Case 1: HDDPC by tracking indoor temperature measurements

The results of the case 1 simulation are shown in Fig. 3-5 and Fig. 3-6. Most of the time, simulated indoor temperature can track a similar

trajectory as the measurement with less cooling load. The sudden increase in indoor temperature on August 11th and 12th was due to a system fault caused by fire alarms. The cooling load reduction was 36.27% on average and 47.25% at maximum. Such a reduction was due to the nature of the predictive control strategy to leverage the thermal inertia of the building and heat loss through the ambient environment. As for indoor air quality, different from the measurement, with the proposed DDPC strategy, the indoor CO₂ concentration never went above the requirement. It also thanks to the nature of the predictive control strategy. Since the occupant schedule was known ahead of time, the DDPC strategy could control the system accordingly to meet the requirements. With a similar temperature trajectory and guarantee of indoor air quality, the DDPC strategy significantly reduced air side coil

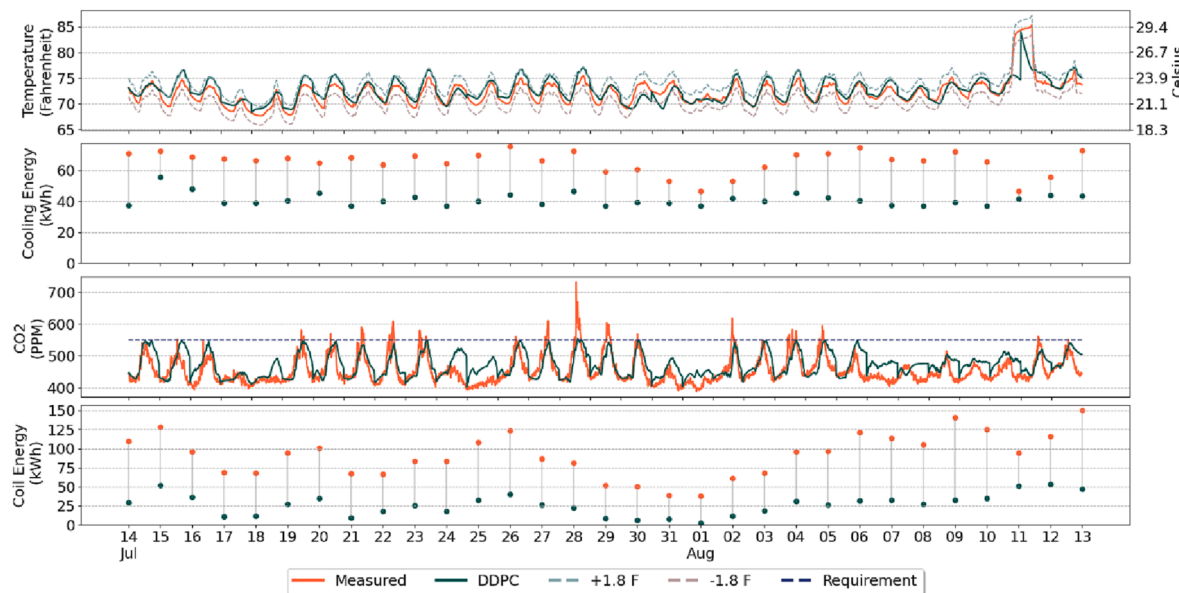


Fig. 3-5. Case 1 simulation results. The plot on the top shows the comparison between simulated and measured indoor temperature. The second plot shows the comparison of cooling energy with/without using DDPC. The third plot shows that comparison between simulated and measured indoor CO₂ concentration. The last plot shows the comparison of coil energy with/without using DDPC.

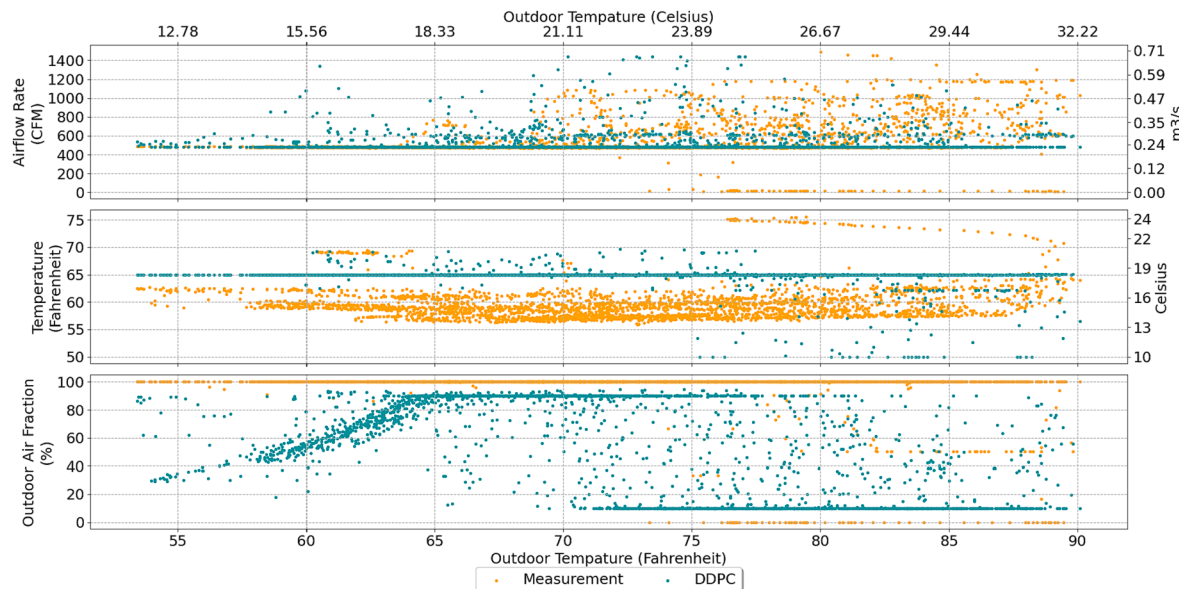


Fig. 3-6. Control inputs of Case 1. Plot show supply airflow rate (top), supply air temperature (middle), and outdoor air fraction (bottom) against outdoor air temperature.

energy usage, as shown in the bottom plot of Fig. 3-5. Two main reasons contributed to such a reduction.

First, except for faulty and minimum airflow rate, most of the measured airflow rate lay in the region of outdoor air temperature between 23.9 and 32.2 °C (75 and 90°F), as shown in the top plot of Fig. 3-6. Differently, most of the simulated temperature lay in the left region of 23.9 °C (75°F) ambient temperature because the DDPC strategy could leverage cool outside air more than the default control strategy. Moreover, compared to the measurement, most of the simulated airflow rates were less than 0.47 m³/s (1000 CFM) due to reduced cooling load.

Second, most of the measured supply air temperatures were between 12.8 and 15.6 °C (55 and 60 °F). It is unnecessary because the measured indoor temperature could be 21.1 °C (70 °F) or even less. However, the most simulated supply air temperature was between 15.6 and 18.3 °C

(60 and 65 °F). The simulated supply air temperature decreased when the outdoor air temperature was more than 23.9 °C (75 °F) to meet the increased cooling demand as shown in the middle plot of Fig. 3-6.

Third, during the test period, the HVAC system operated with a 100% outdoor airflow whatever the outside temperature was. It was to reduce the infection risk of COVID-19, as suggested by CDC [9]. However, with the proposed DDPC strategy, the outdoor air fraction changed dynamically as shown in the bottom plot of Fig. 3-6. Most of the time, the simulated outdoor air fraction lay at maximum (minimum) when the outside air temperature was below 21.1°C/70°F (above 23.9°C/75°F). The fraction in between was either in seeking to meet the required cooling load or indoor air quality.

Therefore, by the combined effect of reduced and shifted airflow rate, increased supply air temperature, and more dynamic outdoor air

Table 4

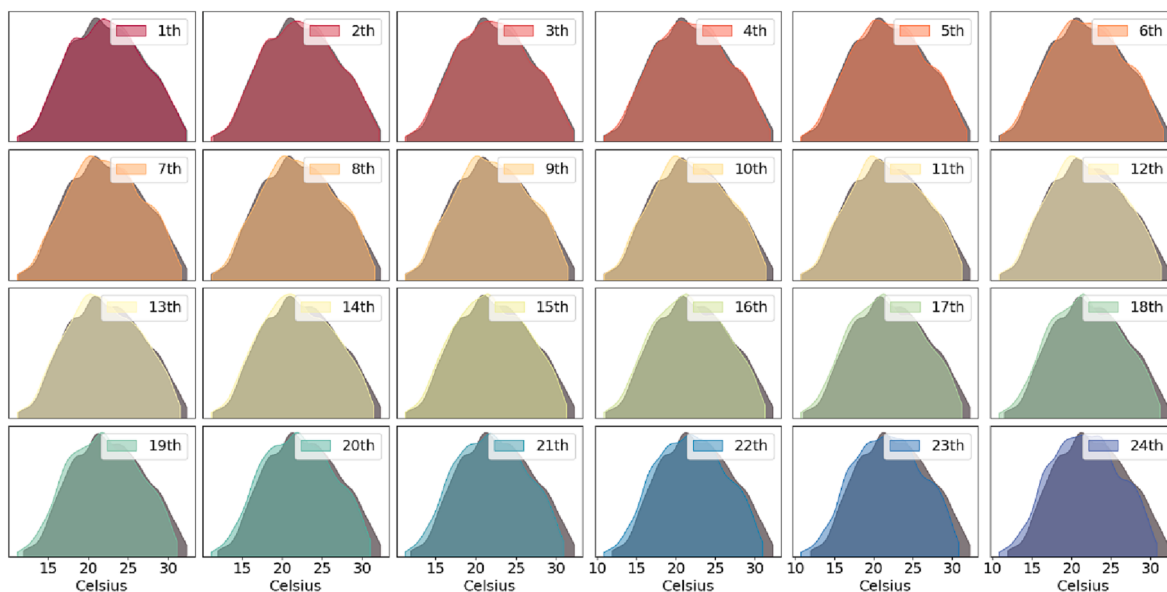
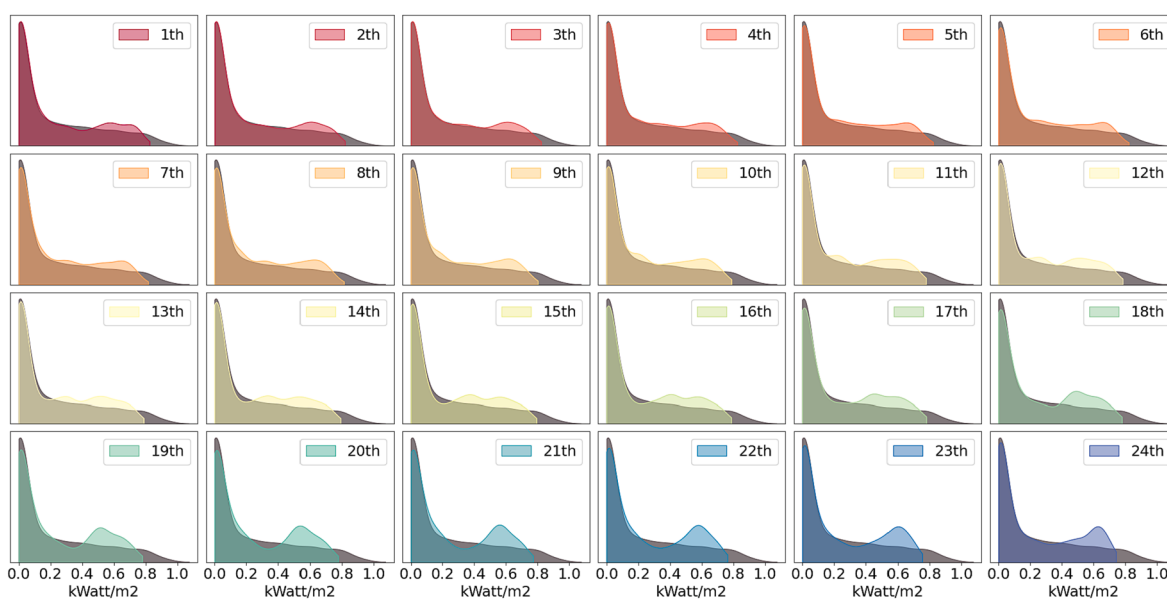
Average MAPE (%) of outdoor temperature forecast of each step during the testing period.

Steps	1	2	3	4	5	6	7	8	9	10	11	12
MAPE	0.722	0.83	1.005	1.195	1.385	1.57	1.775	1.957	2.164	2.349	2.547	2.701
Steps	13	14	15	16	17	18	19	20	21	22	23	24
MAPE	2.887	3.05	3.19	3.363	3.532	3.662	3.784	3.948	4.063	4.219	4.356	4.483

Table 5

Average RMSE of the solar forecast of each step during the testing period.

Steps	1	2	3	4	5	6	7	8	9	10	11	12
RMSE	77.877	85.191	89.381	92.63	95.488	98.668	100.75	101.22	103.01	105.35	107.50	109.44
Steps	13	14	15	16	17	18	19	20	21	22	23	24
RMSE	111.27	112.44	113.66	115.23	116.57	116.63	118.04	119.31	120.90	122.05	123.90	125.51

**Fig. 3-7.** Distributions of outdoor temperature prediction of each time step (colored) and measurement (black).**Fig. 3-8.** Distributions of solar radiation prediction of each time step (colored) and measurement (black).

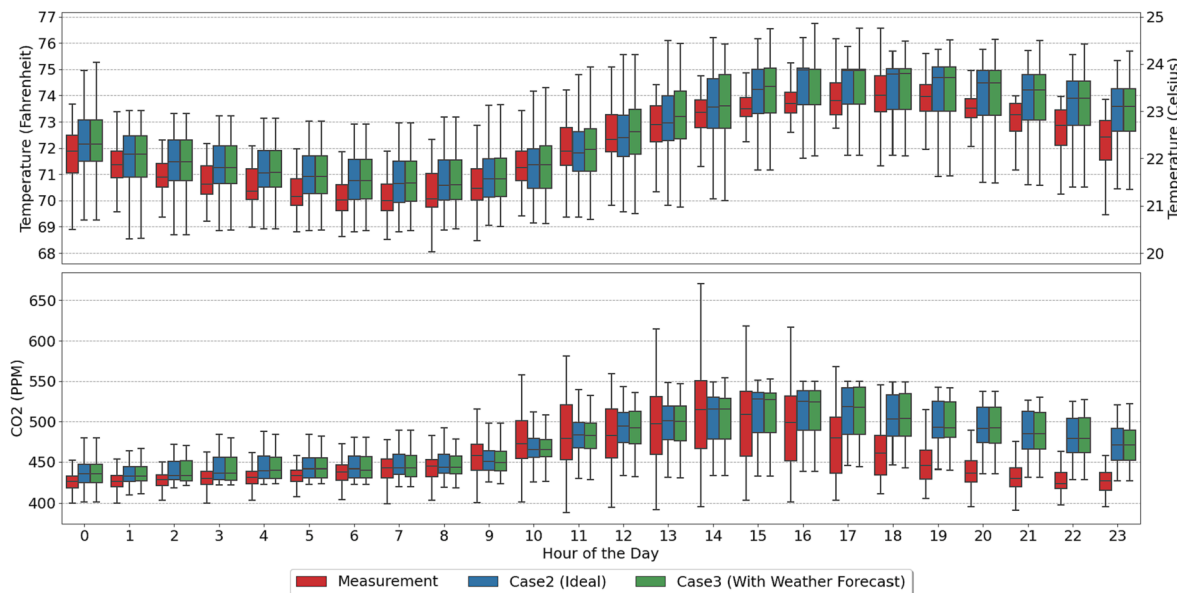


Fig. 3-9. Overall indoor temperature (top) and CO2 concentration (bottom) from measurement (red), Case 2 simulation (blue), and Case 3 simulation (green). (For interpretation of the references to colour in this figure legend, the reader is referred to the web version of this article.)

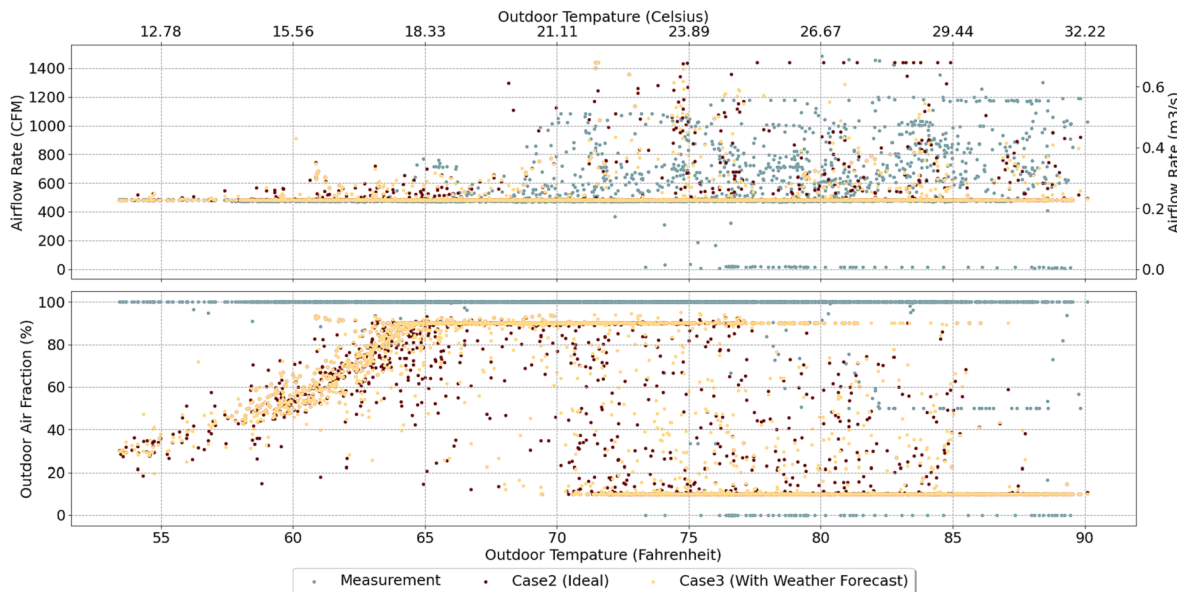


Fig. 3-10. Control inputs of measurement (grey) and Cases 2 (dark red) and 3 (yellow). Plot show supply airflow rate (top) and outdoor air fraction (bottom) against outdoor air temperature. (For interpretation of the references to colour in this figure legend, the reader is referred to the web version of this article.)

fraction, the average air side coil energy reduction over the whole simulation period was 72.72%.

3.2.2. Case 2 & Case 3: Maintaining indoor environmental quality without/with weather forecast

Different from Case 1, Cases 2 and 3 were simulated to evaluate HDDPC's energy reduction potential under pre-defined indoor temperature and CO₂ bounds. The difference between Cases 2 and 3 was without and with actual weather information. The measured weather data was used in Case 2 as an ideal situation, while the weather forecasting was used in Case 3 for a real application situation.

3.2.2.1. Results of weather forecasting. LSTM models were developed for next-6-hour outdoor air temperature and solar radiation forecasts, respectively. After training with 2-year measured data, Table 4 and

Table 5 show the overall performance during the testing period. Both models had the most accurate predictions in the 1st step. The model performances degraded as the prediction time step moved away from the current time step. As shown in Fig. 3-7, the increased error in outdoor air temperature prediction was due to the underestimation of the actual temperature. Such underestimation increased with the increase of prediction steps. On the other hand, as shown in Fig. 3-8, the increased error of solar radiation prediction was due to the overestimation of low solar radiation when the prediction step was more than 12 and the underestimation of the peak solar radiation in all prediction steps. Nevertheless, most prediction results are aligned with the measured data with MAPE less than 4.5%. Therefore, the weather forecast by the proposed LSTM models was used in Case 3.

3.2.2.2. Results of case 2 and 3. For Cases 2 and 3 simulations, the

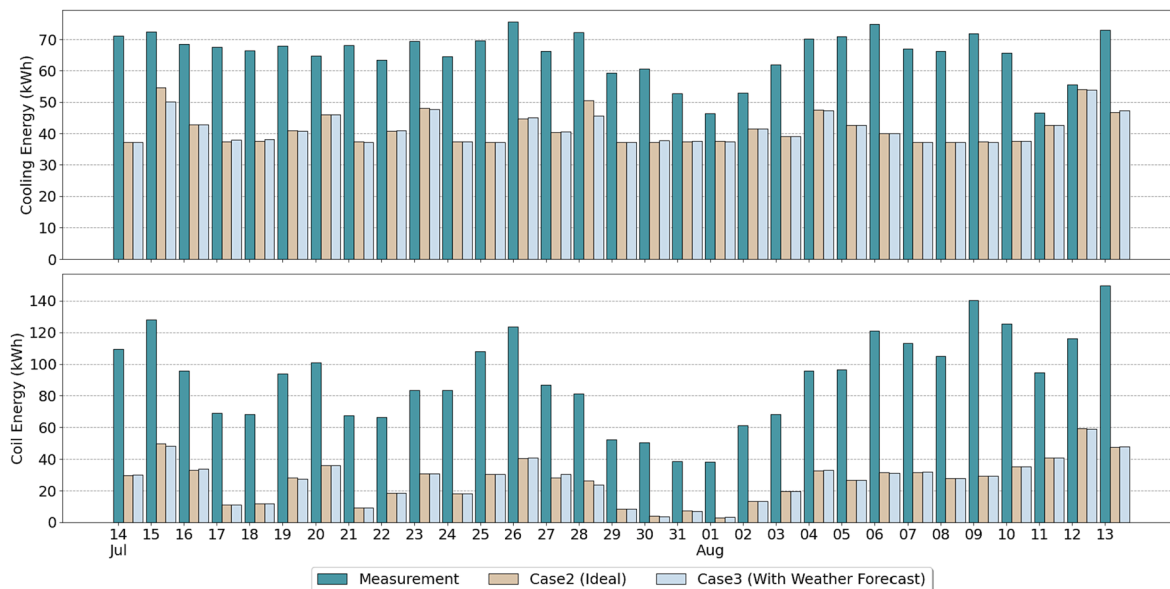


Fig. 3-11. Total cooling energy (top) and airside coil energy (bottom) of measurement (green), Case 2 (brown), and Case 3 (light blue). (For interpretation of the references to colour in this figure legend, the reader is referred to the web version of this article.)

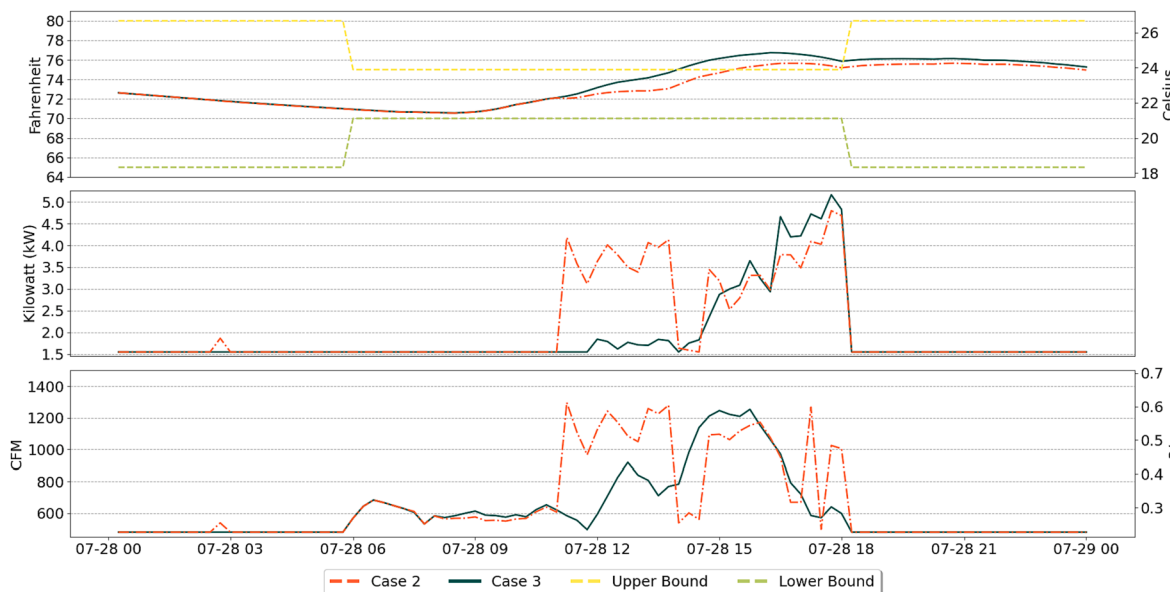


Fig. 3-12. Indoor temperature (top), cooling load (middle), supply airflow rate (bottom) results of cases 2 (red) and 3 (green) on July 28th. (For interpretation of the references to colour in this figure legend, the reader is referred to the web version of this article.)

overall results were shown in Fig. 3-9 and Fig. 3-11, compared with the measurement. The supply air temperature shared a similar behavior to which in Fig. 3-6 and therefore was not shown in detail. Supply airflow rate and outdoor air fraction results were shown in Fig. 3-10. As indicated by the top plot in Fig. 3-9, the simulated temperature was higher than the measurement most time. Because less cooling load was supplied to the room by the room-level controller. Instead of increasing unboundedly, in the late afternoon, the simulated indoor air temperature was fixed at 23.9 °C (75 °F). As for indoor air quality, shown in the bottom plot in Fig. 3-9, at the beginning of each testing day, the simulated indoor CO₂ concentration distribution was similar to the measurement because the room was unoccupied. Differently during the day, the simulated indoor CO₂ concentration was less than 550 PPM, while the measurement sometimes violated the requirement between 11 AM and 5 PM. Comparing Cases 2 and 3, the underestimated weather

conditions caused the insufficient cooling load, which was reflected by a wider interquartile range from 10 AM to 2 PM. Even with a sub-optimal cooling load compared to the ideal Case 2, most indoor temperature from Case 3 was still maintained below 23.9 °C (75 °F) after 2 PM. The indoor CO₂ concentration from Case 3 was similar to which from Case 2. Most time, the concentration could be maintained below the requirement. The exception happened between 2 and 3 PM, in which the concentration was slightly higher than 550 PPM in a small number of time steps. Since the underestimated cooling load from the room-level controller resulted in a reduced total airflow rate and therefore a reduced fresh airflow rate.

As shown in Fig. 3-11, the proposed HDDPC strategy significantly reduced total space cooling load and airside coil energy usage in both Case 2 and Case 3. The average space cooling load reductions were 35.7% and 36%, respectively, for Case 2 and Case 3. The average airside

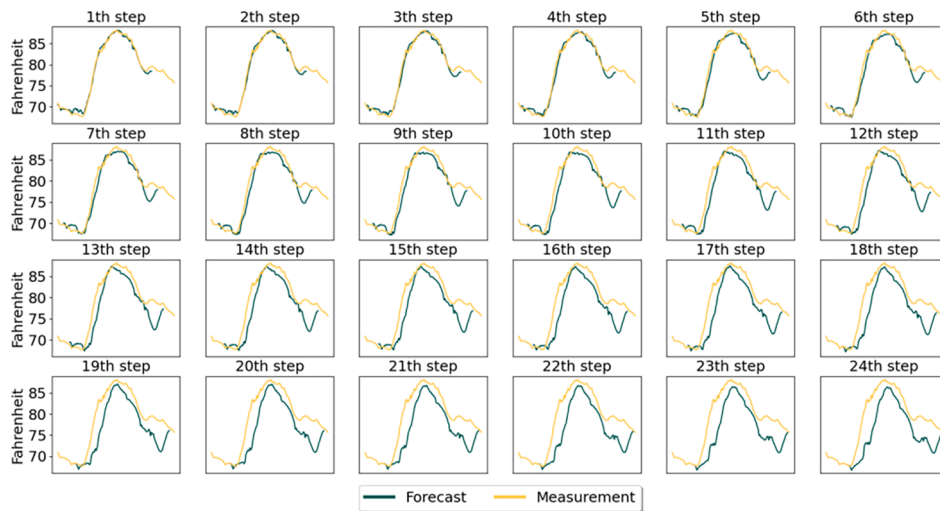


Fig. A1. Outdoor temperature forecast on July 15th.

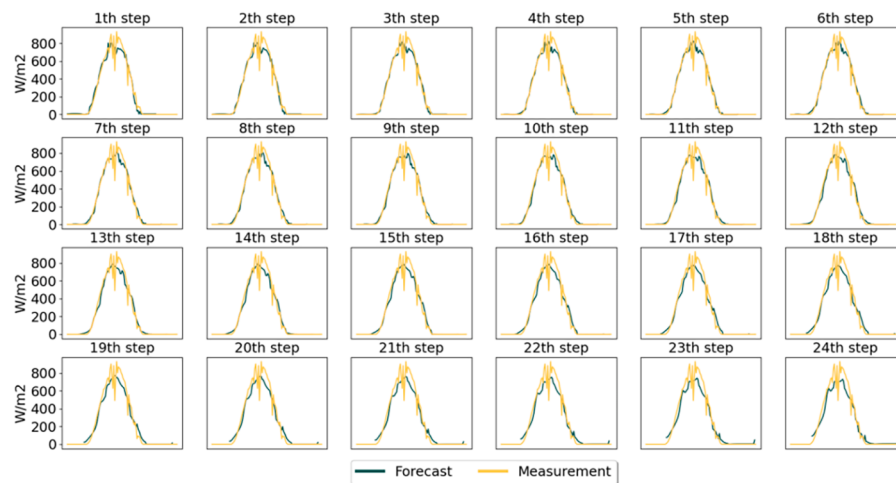


Fig. A2. Solar radiation forecast on July 15th.

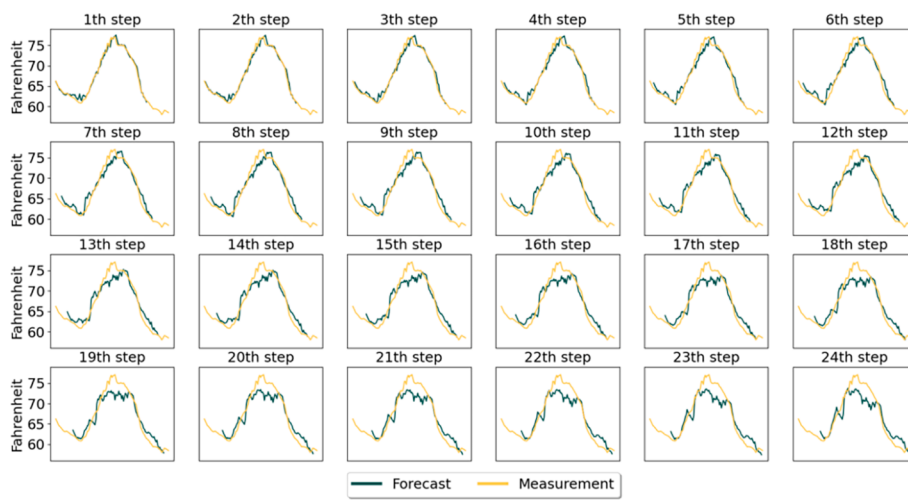


Fig. A3. Outdoor temperature forecast on July 28th.

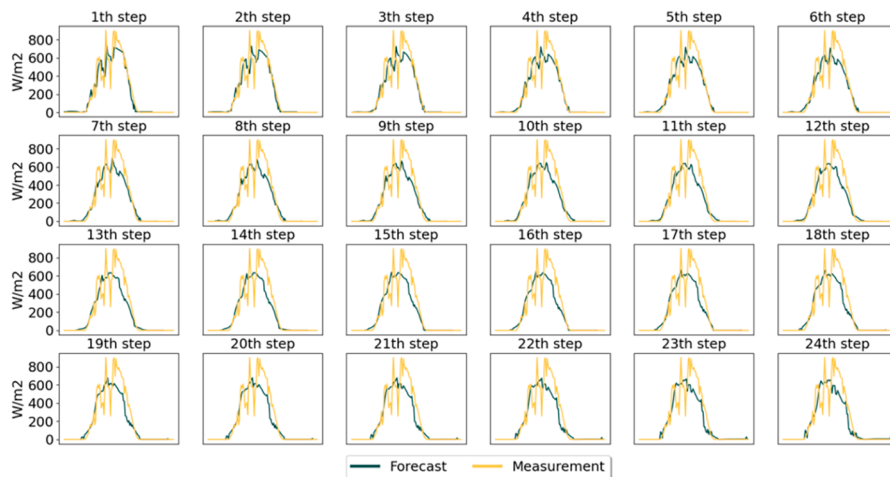


Fig. A4. Solar radiation forecast on July 28th.

coil energy reductions were 72.7% and 72.8%, respectively, for Cases 2 and 3. The cooling energy reduction was due to a lower cooling load supplied at most time steps. The reduced airside coil energy usage was because of the reduced supply airflow rate and more intelligent fresh air intake controls, as shown in Fig. 3–10. The slightly higher reduction from Case 3 somewhat contradicted our intuition that imperfect weather forecasts would cause less energy reduction. However, this can be interpreted as follows.

The most obvious cooling load differences between Cases 2 and 3 can be recognized on July 15 and 28th from Fig. 3–11. On July 15th, the measured maximum outdoor temperature and solar radiation were 25.1 °C (77.1 °F) and 901 W per square meter, respectively, while the forecasted maximums at the 24th step were 23.2 °C (73.7 °F) and 657 W per square meter, respectively. On July 28th, the measured maximum outdoor temperature and solar radiation were 31.2 °C (88.2 °F) and 929 W per square meter, respectively, while the forecasted maximums at the 24th step were 30.2 °C (86.4 °F) and 729 W per square meter, respectively. The time-series weather forecast results were shown in Figs. A1–A4. Such underestimations were also reflected in Figs. 3–7 and 3–8. Due to the underestimated weather conditions, an insufficient cooling load was supplied, resulting in more cooling energy reduction. As a tradeoff, the indoor temperature was increased sometimes to more than 24.4 °C (76 °F), as shown in Figs. 3–9 and Fig. 3–12. On the same two dates, the coil energy differences were not as noticeable as the cooling energy differences. On the one hand, the insufficient cooling load would result in a reduced supply airflow rate, which would reduce the airside coil load. On the other hand, the underestimated weather conditions also limited airflow rate when the outdoor temperature was relatively cool and increased the fresh air intake in the hot period, which would increase the coil load, as shown respectively in Fig. 3–12 around noon and 3:00 PM on July 28th. Also as shown in Fig. 3–10, the outdoor air fraction in Case 3 was at the upper bound more frequently than which in Case 2 when the outdoor temperature was higher than 23.9 °C (75 °F). The combined effect made less difference between Cases 2 and 3 on coil energy usage. Except for these two days, in Case 3, the HDDPC strategy with the proposed weather forecast models had little difference from the ideal case most time.

4. Limitations and future works

Although the proposed HDDPC strategy with weather forecasting provided significant energy reduction on both room and system levels, there were still some limitations that need to be discussed and improved in our future works.

- 1) *Physics-informed loss function:* although the proposed neural network structure was physics-informed, the physics-informed loss function was not used. Due to system faults in the training period, open-loop data was also included in the dataset, therefore richer indoor dynamics were included. The indoor environmental dynamics were learned from historical data and validated in different sanity check cases. In a well-regulated building, open-loop data is hard to obtain. However, we expect including physics-informed terms in the loss function would guarantee the model behavior in such scenarios. One of our future works will be on combining physics-informed model structure with the physics-informed loss function and test in different buildings.
- 2) *Solution feasibility:* in the formulation of optimization problems, although the problems were proven to be convex, the feasibility was not guaranteed due to the hard constraints and uncertainty of weather forecasts. In the simulation studies, the violation of temperature bounds was observed in some time steps. Optimization failures would impede the application of predictive control strategies. The slack variables can be used to allow a small violation of constraints to guarantee feasibility. However, according to [20], slack variables will make state lower bounds non-convex. To facilitate the implementation, make-up controllers can be adopted.
- 3) *Coordination between the room and system:* in the HDDPC strategy, indoor CO₂ concentration was not considered in the room-level controller. In the system-level controller, the fresh air flow rate was dependent on the cooling load from the room-level controller. If the room-level and system-level optimization problems could be solved simultaneously, we would expect a more significant energy reduction. However, based on the simulation results, the solution of a combined problem was highly dependent on the initial guess, which indicates that convexity was not guaranteed. Expertise is needed to directly solve the combined problem. However, an agent-based control policy can be developed and trained based on the proposed models, which will be one of our future works.
- 4) *Impact of occupancy prediction:* occupancy prediction was not considered in this research study because most students in the office were from the same research group and worked based on the schedule. However, for implementations in other buildings, an occupant prediction model will be needed, which will be developed and evaluated in our future research studies.
- 5) *Implementation of the HDDPC strategy:* although the proposed HDDPC strategy achieved significant load reduction and provided good indoor environmental quality in three simulation cases, the implementation into a real building is still necessary to further demonstrate the potential of the proposed HDDPC strategy. For the

implementation, we would expect little or no modification of the proposed methodology, as the control variables are or can be decomposed to writable points in the most BMSs. Therefore, one of our future works will be applying the HDDPC strategy.

5. Conclusion

In this work, we proposed a novel ANN-based physics-informed neural network to facilitate predictive control strategies. The proposed neural network can not only guarantee the time correlation between inputs and outputs but also provide accurate, physics-consistent predictions for indoor temperature and CO₂ dynamics. Incorporating both indoor temperature and air quality considerations into the predictive control strategy, the proposed HDDPC framework optimized the load on both room and system levels and achieved significant load reductions. Developed based on the LSTM structure, two weather forecast models provided short-term, short-time-interval predictions for the outdoor temperature and solar radiation. With the accurate weather forecast model, the HDDPC performance is comparable with the ideal case. The average cooling and airside coil load reductions during the one-month simulation were over 35% and 70%, respectively. To further facilitate data-driven predictive control and demonstrate its performance, physics-informed loss functions, coordinated predictive control, and real building implementation will be future works.

Declaration of Competing Interest

The authors declare that they have no known competing financial interests or personal relationships that could have appeared to influence the work reported in this paper.

Data availability

The data that has been used is confidential.

Acknowledgment

This research was sponsored by Honeywell International Inc.

Appendix

References

- [1] J. Langevin, C.B. Harris, A. Satre-Meloy, H. Chandra-Putra, A. Speake, E. Present, R. Adhikari, E.J. Wilson, A.J. Satchwell, US building energy efficiency and flexibility as an electric grid resource, Joule 5 (8) (2021) 2102–2128, <https://doi.org/10.1016/j.joule.2021.06.002>.
- [2] CBECS 2012: Energy Usage Summary. (n.d.). <https://www.eia.gov/consumption/commercial/reports/2012/energyusage/>.
- [3] Annual Energy Outlook - U.S. Energy Information Administration (EIA). (n.d.). <http://www.eia.gov/outlooks/aoe/>.
- [4] M. Kong, B. Dong, R. Zhang, Z. O'Neill, HVAC energy savings, thermal comfort and air quality for occupant-centric control through a side-by-side experimental study, Appl. Energy 306 (2022), 117987, <https://doi.org/10.1016/j.apenergy.2021.117987>.
- [5] Roth KW, Westphalen D, Llana P, Feng M (2004). The energy impact of faults in US commercial buildings. In: Proceedings of International Refrigeration and Air Conditioning Conference, West Lafayette, IN, USA. <https://docs.lib.psu.edu/cgi/viewcontent.cgi?article=1664&context=iracc>.
- [6] M. González-Torres, L. Pérez-Lombard, J.F. Coronel, I.R. Maestre, D. Yan, A review on buildings energy information: Trends, end-uses, fuels and drivers, Energy Rep. 8 (2022) 626–637, <https://doi.org/10.1016/j.egyr.2021.11.280>.
- [7] N.A. Megahed, E.M. Ghoneim, Indoor Air Quality: Rethinking rules of building design strategies in post-pandemic architecture, Environ. Res. 193 (2021), 110471, <https://doi.org/10.1016/j.envres.2020.110471>.
- [8] X. Lu, Z. Pang, Y. Fu, Z. O'Neill, The nexus of the indoor CO₂ concentration and ventilation demands underlying CO₂-based demand-controlled ventilation in commercial buildings: A critical review, Build. Environ. 218 (2022), 109116, <https://doi.org/10.1016/j.buildenv.2022.109116>.
- [9] Improving Ventilation in Your Home. (2022, June 29). Centers for Disease Control and Prevention. <https://www.cdc.gov/coronavirus/2019-ncov/prevent-getting-sick/improving-ventilation-home.html>.
- [10] Indoor Air Quality in Offices and Other Large Buildings. (2022, February 15). US EPA. <https://www.epa.gov/indoor-air-quality-iaq/indoor-air-quality-offices-and-other-large-buildings>.
- [11] X. Wang, B. Dong, J.J. Zhang, Nationwide evaluation of energy and indoor air quality predictive control and impact on infection risk for cooling season, Build. Simul. 16 (2) (2022) 205–223, <https://doi.org/10.1007/s12273-022-0936-6>.
- [12] Z.Z. He, J.Y. Zhang, F.Y. Zheng, X.J. Jin, Energy-efficiency-oriented optimal control for electrical environmental control system based on advanced neural network, Appl. Therm. Eng. 219 (2023), 119635, <https://doi.org/10.1016/j.applthermaleng.2022.119635>.
- [13] W.H. Chen, F. You, Semiclosed Greenhouse Climate Control Under Uncertainty via Machine Learning and Data-Driven Robust Model Predictive Control, IEEE Trans. Control Syst. Technol. 30 (3) (2022) 1186–1197, <https://doi.org/10.1109/tcst.2021.3094999>.
- [14] J. Drgoña, A. Tuor, E. Skomski, S. Vasish, D. Vrabie, Deep Learning Explicit Differentiable Predictive Control Laws for Buildings, IFAC-PapersOnLine 54 (6) (2021) 14–19, <https://doi.org/10.1016/j.ifacol.2021.08.518>.
- [15] J. Drgoña, A.R. Tuor, V. Chandan, D.L. Vrabie, Physics-constrained deep learning of multi-zone building thermal dynamics, Energy Build. 243 (2021), 110992, <https://doi.org/10.1016/j.enbuild.2021.110992>.
- [16] G. Gokhale, B. Claessens, C. Develder, Physics informed neural networks for control oriented thermal modeling of buildings, Appl. Energy 314 (2022), 118852, <https://doi.org/10.1016/j.apenergy.2022.118852>.
- [17] Gokhale, G. (2022, November 21). PhysQ: A Physics Informed Reinforcement Learning Framework for Building Control. arXiv.org. <https://arxiv.org/abs/2211.11830>.
- [18] L. Di Natale, B. Svetozarevic, P. Heer, C. Jones, Physically Consistent Neural Networks for building thermal modeling: Theory and analysis, Appl. Energy 325 (2022), 119806, <https://doi.org/10.1016/j.apenergy.2022.119806>.
- [19] F. Büning, B. Huber, P. Heer, A. Aboudonia, J. Lygeros, Experimental demonstration of data predictive control for energy optimization and thermal comfort in buildings, Energy Build. 211 (2020), 109792, <https://doi.org/10.1016/j.enbuild.2020.109792>.
- [20] Büning, F. (2020, November 26). Input Convex Neural Networks for Building MPC. arXiv.org. <https://arxiv.org/abs/2011.13227>.
- [21] F. Büning, B. Huber, A. Schalbetter, A. Aboudonia, M. Hudoba de Badyn, P. Heer, R.S. Smith, J. Lygeros, Physics-informed linear regression is competitive with two Machine Learning methods in residential building MPC, Appl. Energy 310 (2022), 118491, <https://doi.org/10.1016/j.apenergy.2021.118491>.
- [22] F. Büning, J. Warrington, P. Heer, R.S. Smith, J. Lygeros, Robust MPC with data-driven demand forecasting for frequency regulation with heat pumps, Control Eng. Pract. 122 (2022), 105101, <https://doi.org/10.1016/j.conengprac.2022.105101>.
- [23] F. Arnold, R. King, State-space modeling for control based on physics-informed neural networks, Eng. Appl. Artif. Intel. 101 (2021), 104195, <https://doi.org/10.1016/j.engappai.2021.104195>.
- [24] S. Yang, M.P. Wan, W. Chen, B.F. Ng, S. Dubey, Model predictive control with adaptive machine-learning-based model for building energy efficiency and comfort optimization, Appl. Energy 271 (2020), 115147, <https://doi.org/10.1016/j.apenergy.2020.115147>.
- [25] Z. Deng, X. Wang, Z. Jiang, N. Zhou, H. Ge, B. Dong, Evaluation of deploying data-driven predictive controls in buildings on a large scale for greenhouse gas emission reduction, Energy 270 (2023), 126934, <https://doi.org/10.1016/j.energy.2023.126934>.
- [26] P. Li, D. Vrabie, D. Li, S.C. Bengea, S. Mijanović, Z.D. O'Neill, Simulation and experimental demonstration of model predictive control in a building HVAC system, Sci. Technol. Built Environ. 21 (6) (2015) 721–732, <https://doi.org/10.1080/23744731.2015.1061888>.
- [27] M. Fiorentini, J. Wall, Z. Ma, J.H. Braslavsky, P. Cooper, Hybrid model predictive control of a residential HVAC system with on-site thermal energy generation and storage, Appl. Energy 187 (2017) 465–479, <https://doi.org/10.1016/j.apenergy.2016.11.041>.
- [28] H. Huang, L. Chen, E. Hu, A new model predictive control scheme for energy and cost savings in commercial buildings: An airport terminal building case study, Build. Environ. 89 (2015) 203–216, <https://doi.org/10.1016/j.buildenv.2015.01.037>.
- [29] A. Khakimova, A. Kusatayeva, A. Shamshimova, D. Sharipova, A. Bemporad, Y. Familiant, A. Shintemirov, V. Ten, M. Rubagotti, Optimal energy management of a small-size building via hybrid model predictive control, Energ. Buildings 140 (2017) 1–8, <https://doi.org/10.1016/j.enbuild.2017.01.045>.
- [30] J. Drgoña, D. Picard, L. Helsen, Cloud-based implementation of white-box model predictive control for a GEOTABS office building: A field test demonstration, J. Process Control 88 (2020) 63–77, <https://doi.org/10.1016/j.jprocont.2020.02.007>.
- [31] C. Finck, R. Li, W. Zeiler, Economic model predictive control for demand flexibility of a residential building, Energy 176 (2019) 365–379, <https://doi.org/10.1016/j.energy.2019.03.171>.
- [32] T. Hilliard, L. Swan, Z. Qin, Experimental implementation of whole building MPC with zone based thermal comfort adjustments, Build. Environ. 125 (2017) 326–338, <https://doi.org/10.1016/j.buildenv.2017.09.003>.
- [33] J. Joe, P. Karava, A model predictive control strategy to optimize the performance of radiant floor heating and cooling systems in office buildings, Appl. Energy 245 (2019) 65–77, <https://doi.org/10.1016/j.apenergy.2019.03.209>.

- [34] D. Sturzenegger, D. Gyalistras, M. Morari, R.S. Smith, Model Predictive Climate Control of a Swiss Office Building: Implementation, Results, and Cost-Benefit Analysis, *IEEE Trans. Control Syst. Technol.* 24 (1) (2016) 1–12, <https://doi.org/10.1109/tcst.2015.2415411>.
- [35] R. De Coninck, L. Helsen, Practical implementation and evaluation of model predictive control for an office building in Brussels, *Energ. Buildings* 111 (2016) 290–298, <https://doi.org/10.1016/j.enbuild.2015.11.014>.
- [36] D. Blum, Z. Wang, C. Weyandt, D. Kim, M. Wetter, T. Hong, M.A. Piette, Field demonstration and implementation analysis of model predictive control in an office HVAC system, *Appl. Energy* 318 (2022), 119104, <https://doi.org/10.1016/j.apenergy.2022.119104>.
- [37] Z. Pang, F. Niu, Z. O'Neill, Solar radiation prediction using recurrent neural network and artificial neural network: A case study with comparisons, *Renew. Energy* 156 (2020) 279–289, <https://doi.org/10.1016/j.renene.2020.04.042>.
- [38] T.T.K. Tran, S.M. Bateni, S.J. Ki, H. Vosoughifar, A Review of Neural Networks for Air Temperature Forecasting, *Water* 13 (9) (2021) 1294, <https://doi.org/10.3390/w13091294>.
- [39] M.J.D. Powell, A Direct Search Optimization Method That Models the Objective and Constraint Functions by Linear Interpolation, in: S. Gomez, J.-P. Hennart (Eds.), *Advances in Optimization and Numerical Analysis*, Springer Netherlands, Dordrecht, 1994, pp. 51–67.
- [40] RESET® Standard. (n.d.-c). <https://www.reset.build/standard/air>.